Research Article

Journal of Geophysical Research: Oceans
DOI 10.1002/2016JC012241

A tale of two eddies: The bio-physical characteristics of two contrasting cyclonic eddies in the East Australian Current System

M. Roughan[1,2], S. R. Keating[1], A. Schaeffer [1,2] , P. Cetina Heredia[1,2], C. Rocha[1], D. Griffin[3], R. Robertson[4,2], I.M. Suthers[5,2].

[1]Coastal and Regional Oceanography Lab, School of Mathematics and Statistics UNSW Australia, Sydney, NSW, 2052 Australia. [2]Sydney Institute of Marine Science, Mosman NSW 2088. Australia.[3]CSIRO Marine and Atmospheric Research Hobart Tasmania.[4]UNSW Canberra. [5]School of Biological Earth and Environmental Sciences, UNSW Australia.

Corresponding author: Moninya Roughan (mroughan@unsw.edu.au)

Key Points:

- We contrast a suite of 3-D observations of a cyclonic frontal eddy (~ 35 km), and a mesoscale cyclonic eddy (~160 km) in the Tasman Sea
- The frontal eddy was short lived (~ 4 weeks), deep (~1000 m), highly ageostrophic, and dynamic. Both eddies were tilting
- Both eddies were productive, however the productivity of the frontal eddy which formed on the shelf was proportionately higher

Received: Aug 12, 2016; Revised: Feb 06, 2017; Accepted: Feb 12, 2017

Abstract

Mesoscale cyclonic eddies are known to be highly productive. Less well-known are the dynamics and productivity of smaller cyclonic eddies, known as *frontal eddies*, that form on the landward side of western boundary currents. In this study we investigate the physical and biogeochemical properties of two contrasting cyclonic eddies in the East Australian Current (EAC). The first ("Murphy"), a mesoscale cyclonic eddy that formed at ~28°S with a diameter of ~160 km and high surface chlorophyll-*a* concentrations, which lived ~47 days. The second ("Freddy"), a smaller frontal eddy (~35 km diameter) that formed from a shelf water billow ~7 days prior to sampling at ~31.5°S and was advected off the shelf along the EAC front (from ~200m to 4000m of water). Both eddies were at least 1000m deep with a similar steric height anomaly. We introduce and employ 'the method of closest approach' using shipboard ADCP velocities to estimate the eddy centers, which reveals significant tilting through the water column. We estimate rotation rates of 4-10 days and 1-9 days and Rossby numbers 0.25-0.1 and 0.6-0.1, from the surface to 600m for Murphy and Freddy respectively. High-resolution altimetry measurements from the SARAL/AltiKA satellite provide estimates of the ageostrophic component of rotation. Our results show that the frontal eddy is significantly more ageostrophic, energetic and productive than the mesoscale cyclone, despite its small size and short life (~4 weeks). We suggest that frontal eddies have potential to contribute significantly to the net productivity of the Tasman Sea region.

1 Introduction

Western Boundary Currents and Mesoscale Eddies

Energetic mesoscale eddies with diameters of 100 - 200 km are ubiquitous features of the global ocean. Many propagate westward across ocean basins (Chelton 2011a, 2011b). In western boundary currents (WBCs), they transport mass, heat, and salt poleward from the equator (McGillicudy et al., 2007, Zhang, et al. 2014). In addition, they have the potential to retain and advect nutrients (Bakun 1996, Benitez-Nelson et al. 2007), seed and grow populations of biological organisms (McGillicuddy et al. 1999) and have been shown to generate new production (Gaube et al. 2013), if sufficiently long lived.

Eddy formation and shedding mechanisms have been openly debated; however, there is a consensus that mesoscale eddies in WBCs form initially from meanders in the flow, becoming increasingly unstable through barotropic and baroclinic instabilities that propagate in WBCs (e.g. Bowen et al. (2005), Stammer (1997), Mata et al. (2006)). Eddies form and shed due to the transfer of mean energy from the jet to eddy kinetic energy (e.g Rubio et al. 2009, Macdonald et al. 2016). In baroclinic flows, mean potential energy is transferred due to density-driven differences while mean kinetic energy from horizontal shear is transferred in barotropic flows. In other parts of the global ocean mesoscale eddies are also generated through wind stress curl, or flow topography interactions (e.g in the lee of the Hawaiian islands, Yoshida et al. (2010)).

Eddies in the East Australian Current System

The East Australian Current (EAC) is the WBC of the south Pacific subtropical gyre, transporting heat from the tropics down the east coast of Australia to the Tasman Sea, where it separates, typically at ~ 32°S (Cetina Heredia et al. 2014, Figure 1a). Eddy shedding can occur at any latitude, however it typically occurs when the EAC jet extends poleward, and subsequently separates, resulting in a rapid retraction of the EAC separation latitude after eddy shedding (Cetina Heredia et al. 2014).

Eddy shedding in the EAC has been studied using a range of tools including SSH (Bowen et al. 2005), a numerical model forced with climatology (Wilkin and Zhang 2007), a moored timeseries (Mata et al. 2006) and standard shipboard observations (Ridgway et al. 2008). Each of these studies shows a peak in eddy shedding frequency of ~90 - 120 days. These periodic fluctuations in the EAC extension and eddy shedding adjacent to the continental shelf of SE Australia have been shown to drive shelf circulation (Wood et al. 2016) and to correlate with the onshore transport of cold nutrient-rich bottom water at the shelf break (Schaeffer et al. 2014) thereby contributing to the productivity of shelf waters.

Both cyclonic and anti-cyclonic eddies are prolific in the EAC System, particularly downstream of the EAC separation point between 32-39°S (Everett et al. (2012)). In this region, eddies have increased anomalies of sea level, surface temperature and surface chlorophyll *a* (chl. *a*), and are associated with faster rotation rates (Everett et al. 2012, 2014). Using the Chelton et al. (2011a, 2011b) eddy database, Everett et al. (2012) showed that Tasman Sea eddies range in diameter from 100 - 300 km with a mean of ~ 185 km in our region, with a mean sea level anomaly of ~ 0.23 - 0.24 m, and a density of approximately 17 eddies in the region per day. Direct observations of the vertical structure of mesoscale cyclonic and anti-cyclonic eddies using more than 2500 Argo float profiles showed radii of 100 - 200 km, with sea level anomalies of ~0.4 m at the core, and a depth extending to at least 1000 m (Rykova and Oke, 2015). While Everett et al (2012) found no significant difference in the abundance, diameter or amplitude of cyclonic versus anti-cyclonic eddies in the Tasman Sea, Oke and Rykova (2015) showed that anti-cyclones were consistently larger and deeper than cyclones. This discrepancy may be an artifact of the different methodologies used to detect and measure the eddies.

Frontal Eddies

Smaller cyclonic eddies have been observed forming at the front between a WBC and adjacent waters, especially on the landward side of the jet where the lateral buoyancy gradient is greater and the bottom topography shallower. Known as 'frontal eddies', they have been observed in the Kuroshio, (Kimura et al. 1997, Kasai et al. 2002), the Gulf Stream (Lee et al. 1991), and the EAC (Schaeffer et al. Sub.). Typically frontal eddies form frequently (at least occurring approximately every 2 weeks), they range ~ 10 – 60 km in diameter and are short lived, lasting 1 - 4 weeks.

A typical frontal eddy starts its life as an instability along the inshore edge of the WBC, e.g. as a submesoscale billow, meander or filament of water that streams from the poleward flowing jet (Gula et al. 2016, Schaeffer et al Sub.). We note that various definitions of submesoscale exist based on

length scale (McWilliams 2016) and Rossby number and Richardson number (Thomas et al. 2008, 2013). Here we use the dynamical definition of Thomas et al. (2008) and Hetland (2016) where submesoscale flows are characterized by high Rossby number or low Richardson number. Frontal eddies can grow through a combination of wind forcing, where a sudden reversal in the wind direction from poleward to equatorward provides surface momentum along the western edge of the billow (Schaeffer et al. Sub.) and a subsequent transfer of energy from the jet to the billow (Macdonald et al. 2016). In an idealized numerical modeling study, Macdonald et al. (2016) showed that equatorward downwelling-favourable winds drive the deepest cyclonic rotation in the smaller cyclonic eddies that form from barotropic instability at or on the narrow EAC shelf. In the Gulf Stream frontal eddies can be driven by both barotropic conversion from mean to eddy kinetic energy, through horizontal Reynolds stress, and baroclinic conversion from eddy potential to eddy kinetic energy through vertical eddy fluxes of buoyancy (Gula et al. 2015).

Productivity in Cyclonic Eddies

Cyclonic eddies are known to be upwelling favorable in their core through vertical eddy pumping in the interior, thus resulting in the colder core compared to the water around them. In addition, there are a number of more complex mechanisms that contribute to uplift within mesoscale cyclonic eddies that may result in an increase in productivity and drive the distribution of chlorophyll *a* around an eddy. These include eddy-Ekman pumping which is an interaction between the rotating eddy and the prevailing wind (McGillicuddy et al. 2007), eddy advection of meridional property gradients around an eddy (Chelton et al. 2011a) and submesoscale pumping around the edges of the eddy (Siegel et al. 2011, Mahadevan et al. 2012, Gaube et al. 2015).

Chlorophyll *a* concentrations estimated from satellite-derived ocean color are considerably higher in cyclonic eddies than anti-cyclonic eddies that form in WBC regions (Gaube et al. 2014). Indeed, in the Tasman Sea region, Everett et al (2012) found that, mesoscale cyclonic eddies have almost double the surface chl. *a* (0.35 mgm^{-3}) concentrations of anti-cyclonic eddies.

As with mesoscale eddies, frontal eddies can also become more productive through upwelling of nutrient-rich water in their core. Yoder et al. (1981) and Lee et al. (1991) showed that upwelling within frontal eddies in the Gulf Stream is an important mechanism sustaining biological productivity, including phytoplankton and zooplankton growth. Lee et al. (1991) showed that frontal eddies in the Gulf Stream lifted isotherms at a rate of approximately 10 m d^{-1}, upwelling nutrients into to the euphotic zone to stimulate phytoplankton growth. More recently, Gula et al. (2016) hypothesized that submesoscale dynamics within frontal eddies could potentially impact biological production by further increasing the supply of nutrients in the surface layer.

Continental Shelf Entrainment

It has previously been shown that entrainment of continental shelf waters is an important cross shelf transport mechanism that can contribute to the offshore movement of nutrients, fish eggs and seed populations of larval fish. In the California Current system, Nagai et al. (2015) showed that

cyclonic, and to a lesser degree, anti-cyclonic (mesoscale) eddies were significant in the transport of carbon and nutrients from the shelf many hundreds of kilometers offshore. Specifically they identified the tendency for cyclonic eddies to trap cold, previously upwelled water, laden with nutrients and organic matter, in contrast to the anti-cyclonic eddies, which had lower nutrient concentrations and less organic matter.

In the Kuroshio entrainment of coastal water into a frontal eddy has been shown to result in an increased concentration of chl. *a* (Kasai et al. 2002), supported by upwelling at the core of the eddy. In addition, the frequent encroachment of cyclonic eddies onto the continental shelf was shown to contribute to on-going enrichment. In the EAC, Macdonald et al. (2016) and Everett et al. (2015) showed that a frontal eddy was able to entrain large volumes of shelf waters, thus increasing the potential for higher nutrient concentrations and seed populations, (Deibel and Paffenhoffer, 2009). Kasai et al. (2002) concluded that the entrainment process is essential for the survival and recruitment of larval fish in the Kuroshio system.

Despite their obvious high productivity, little is known about the dynamics and the hydrography of frontal eddies. Moreover, little is known about the coupled physical and biogeochemical processes occurring in frontal eddies and their contribution to overall productivity in typically oligotrophic western boundary currents. It is only in recent times that technology has advanced to the point that we can observe (e.g. Schaeffer et al. Sub.), model (Macdonald et al. 2016), track, and measure small scale eddies with some degree of precision.

In this study we present results from a research voyage aboard the RV Investigator, dedicated to investigating the physical and biogeochemical properties of two contrasting cyclonic eddies in the Tasman Sea. The first eddy, affectionately named Eddy Murphy, was a large mesoscale cyclonic eddy with a diameter of ~160 km that formed adjacent to the continental shelf at ~ 28^{o}S along the landward front of the EAC, nearly four weeks before we sampled it. The second eddy was a smaller frontal eddy, affectionately named Freddy, with a diameter of ~35 km, that formed on the continental shelf from a shelf water billow at ~ 31.5^{o}S approximately 7 days before we sampled it. Observational datasets depicting the 3-D structure of eddies are rare, and to date the dynamics of frontal eddies have primarily been diagnosed through modeling studies (e.g Gula et al. 2016 in the Gulf Stream). Our comprehensive data set revealing the 3-D structure and dynamics of two contrasting cyclonic eddies shows that not all cyclonic eddies are created equal, i.e. the smaller frontal eddy is significantly more ageostrophic, energetic and productive than the mesoscale cyclone, despite its small size and short life. We suggest that frontal eddies may contribute significantly to the net productivity of the Tasman Sea region.

2 Observational Methods

2.1 Satellite Observations

We make use of satellite remote sensed observations of AVHRR and MODIS sea surface temperature (SST) and ocean color on cloud-free days, processed and served through the IMOS

ocean current facility, www.oceancurrent.imos.org.au. A 3-day composite image of SST and geostrophic velocities from gridded altimetry centered on 07 June 2015 (Figure 1a) shows the warm water of the EAC flowing southward past Brisbane and eastward around a large cyclonic eddy. Also visible is a small dip in SST off the coast at 32.75°S representing the frontal eddy, however this is eddy is not resolved by the geostrophic velocities.

The first evidence of Freddy appears in SST imagery from 2 June (Sup. Mat. Figure S1). The image (not shown) reveals a cold circular surface feature on the continental shelf at (~31.5°S) in < 200 m of water. This was 7 days before we first sampled the eddy on 9 June (Table 3, 4). The first evidence of Eddy Murphy appears in the SST imagery at 28°S on 9 May. At the time of sampling (4 June 2015) Murphy was ~ 26 days old (Table 3,4). Both eddies are evident in the SST (Figure 1b) and ocean color images (Figure 1 c) around the time of sampling (5 June Murphy and 9 June Freddy).

Due to its small size, at no time is there any evidence of Freddy in SSH imagery from AVISO. However, purely serendipitously the SARAL satellite (Indian Space Research Organisation and CNES France) mounted with an AltiKa altimeter made a pass directly through both eddies concurrent with our in-situ sampling on 4 June and 8 June. The SARAL/AltiKa mission is the first Ka–band altimetric mission dedicated to oceanography with a very high along-track resolution and small footprint (5.7 km as opposed to 9.6 km for Jason-2 altimeter) (Valladeau et al. 2015) and sea-surface height RMS of 3.4 cm (Verron et al. 2015). To our knowledge this is the first concurrent in-situ and high-resolution altimetry observations of a frontal eddy.

2.2 In-situ Observations

Oceanic eddies are ubiquitous but are difficult to study because they are generally ephemeral and evolve too quickly to be easily and repeatedly located, tracked and sampled (Dickey 2008). This problem is considerably amplified when locating and sampling smaller (submesoscale) eddies. We use a series of observations from a 16 day research cruise during the Austral Winter (2 - 18 June 2015) aboard the Australian Marine National Facility RV Investigator (http://www.csiro.au/en/Research/Facilities/Marine-National-Facility). Standard shipboard measurements were taken including: underway thermosalinograph (TSG), with an intake at a depth of 7.9m located on the drop keel; underway shipboard acoustic Doppler current profiles (S-ADCP) from an RDInstruments OS75Khz initially, which was replaced by an RDInstruments OS150khz (on 12 June 07h) after the first ADCP failed (on 11 June 21h), with depth ranges of ~820 m and ~330 m and bin sizes of 16m and 8m, respectively; and vertical CTD profiles of conductivity, temperature, pressure, fluorescence, dissolved oxygen, PAR and transmissivity, taken at 48 stations to a maximum depth of ~1000 m (Table 1). CTD data were QC'd and processed to NetCDF format by CSIRO using their standard procedures. The CTD was mounted on an SBE32, 24 x 10L bottle rosette sampler. Multiple water samples were typically taken at approximate depths of 5:25:100, 200, 300, 500 and 1000 m for biogeochemical analyses including measurements of nutrients, dissolved oxygen, chlorophyll extraction, and a suite of carbon chemistry data detailed in companion papers. Fluorescence voltages were converted to chl. *a* concentrations (mg m^{-3}) through regression analysis, with an $R^2 = 0.81$ using extracted values of chl. *a* (66 points). The key CTD stations used in this

paper are along two transects, the first from west to east in Murphy (stations 8-13, Figure 1d), the second from south-north in Freddy (Stations 23,24,22,25,26, Figure 1e). To enable comparison with historic observations we present salinity as the unitless practical salinity (S) rather than using the TEOS-10 Absolute Salinity scale. However we use the TEOS-10 toolbox (McDougall and Barker 2011) to calculate density and other hydrographic properties.

A lowered ADCP (L-ADCP) system was mounted on the CTD rosette, consisting of RDInstruments 150kHz downward (WHM150) and 300kHz upward (WHM300) looking ADCPs. Horizontal velocities were obtained using the processing software developed by Thurnherr (2010). Typical uncertainties in the horizontal velocities are ≤ 3 cm s^{-1} (Thurnherr, 2010). However, our uncertainties may be higher as few of the profiles were full depth, and we used a 150kHz LADCP instead of the 300kHz.

In addition to the standard shipboard observations, a key piece of instrumentation was a vertically profiling towed body called a Triaxus. The Triaxus was towed at a speed of 8 knots, at a distance of approximately 1200 m behind the vessel, while profiling from the surface to depths of 150 – 200 m. Horizontal spacing between vertical CTD casts was approximately 900 - 1500 m. The Triaxus was fitted with a CTD (conductivity, temperature, pressure, fluorescence, dissolved oxygen and transmissivity) and a laser optical plankton counter to measure the particle size spectrum in the water column, including biomass and biovolume. All data was sent to the vessel via a fiber optic cable in real time. Unfortunately the vehicle was lost at sea (on 13 June 07h), thus no post voyage calibrations were performed.

We deployed 10 Surface Velocity Program drifters throughout the campaign, generously provided by the NOAA global drifter program (Sup. Mat. Table S1). Each drifter was drogued at a mean depth of 15 m. We used the drifters as a way of tracking the eddies and subsequently helping to identify some of the physical characteristics of the eddies.

3 The Needle in the Haystack: Finding Frontal Eddies

The smaller and more transient the eddy is, the more difficult it is to find and track. While mesoscale eddies are easily visible on altimetry, frontal eddies are not generally visible in SSH estimates (because of the wide spacing and infrequently-sampled tracks). Moreover, frontal eddies are typically not resolved in 'eddy' permitting (~10 km resolution) models such as Bluelink (e.g. Schiller et al. 2008) or OFES (Masumoto et al., 2004). To aid in eddy detection, we developed a high-resolution (~2 km) ocean ensemble forecast for the duration of the cruise, however frontal eddy formation and evolution was inconsistent in the ensemble simulations and thus the model was unhelpful in the real time eddy tracking (which is the subject of ongoing modelling work). Thus we were reliant upon cloud free remote sensed SST information for eddy detection alone. Initially near-real-time SST imagery was used to identify candidate eddies off the east coast of Australia from 27 - 34°S. Cyclonic eddies were distinguished by a cold temperature anomaly at the surface that persisted for several days.

3.1 Eddy Detection Algorithm

Once a cyclonic eddy had been identified from satellite imagery of SST and the RV Investigator had transited into the interior of the eddy, ADCP measurements of upper ocean currents (1 - 2 ADCP bins) were used to estimate the location of the eddy center. Following Nencioli et al. (2008), ADCP velocity measurements were projected onto a cylindrical coordinate system centered at a test point, giving the radial and tangential velocity components about the test point for each ADCP measurement. We then calculated the mean tangential velocity and mean radial velocity (averaged over the most recent ADCP velocity measurements) with respect to the test point. This was repeated for a grid of test points, resulting in maps of the mean tangential and radial velocities about each point on the grid (Figure 2). Note that these maps refer to the mean radial and tangential velocity *about* a point, not *at* a point. Thus, the eddy center was identified as the test point about which the tangential velocity was maximum and the radial velocity was zero.

We found this approach to be an effective means of finding and tracking eddies while underway. One strength of the method is that the eddy center estimate can be improved or updated as more ADCP data becomes available. This was particular useful in the case of the frontal eddy because of its small size and rapid translational velocity and because of the presence of cloud cover in the latter part of the cruise, which precluded the use of SST imagery to track the eddy.

The eddy center detection algorithm of Nencioli et al. (2008) also allowed on-the-fly estimates of eddy properties such as vorticity, radius and eddy tilt (see below) that were useful for adapting the sampling strategy while underway. The eddy vorticity and radius were estimated by plotting the tangential velocity, V_T, against the distance from the eddy center, r. For a uniform vorticity flow, the tangential velocity is expected to increase as $V_T = \Omega r$, where Ω is the vorticity of the eddy. The eddy vorticity was estimated from the slope of the graph, while the eddy radius was estimated as the radius at which the tangential growth no longer grows linearly with distance from the eddy center.

3.2 Method of Closest Approach

Despite its usefulness in the field, the Nencioli et al. (2008) eddy detection algorithm was not accurate enough for detailed analysis of eddy properties. It is not clear how to estimate the error in the method, and it is plausible that several biases could impact the results. First, the eddy center is identified as the point with maximum mean tangential velocity. Because the tangential velocity increases with distance from the eddy center, the result will be weighted more towards data from the edge of the eddy and less towards data near the center, where velocities are smaller. The size of the larger, northern eddy was also an issue because the eddy center could move appreciable distances in the time taken to transect a significant fraction of the eddy diameter. And estimates of the eddy vorticity and radius assume a uniform vorticity flow, which will not be appropriate if the eddy is elliptical, asymmetric, or undergoes differential rotation due to interactions with the wind field, ocean floor, or adjacent currents like the EAC.

To address these issues, a more direct method of estimating the eddy center location was developed based upon decomposing the ADCP currents into longitudinal (along-track) and normal (across-track) components. As the ship passes the point of closest approach to the eddy center, the normal component of the measured current will change sign, indicating that the eddy center lies along a line orthogonal to the point of closest approach.

From simple geometric arguments, the normal and longitudinal components of the velocity are related to the tangential velocity around the eddy by, respectively, $V_N = V_T \sin\alpha$ and $V_L = V_T \cos\alpha$, where α is the angle subtended by the ship as it travels along a straight line (Figure 3a). If r_0 is the distance of closest approach and ℓ is the distance measured from this point along the ship track then the distance of the ship from the eddy center will be $r = \sqrt{\ell^2 + r_0^2}$. (Note that we ignore the effect of curvature of Earth's surface on these scales.) Thus, $\sin\alpha = \ell/r$ and $\cos\alpha = r_0/r$. Finally, if the velocity field in the core of the eddy is a uniform vorticity flow (a reasonable assumption near the eddy center) then $V_T = \Omega r$ and the normal and longitudinal velocity components are

$$V_N = \Omega\ell, \;\; V_L = \Omega r_0.$$

The implication is that the point of closest approach along the ship track ($\ell = 0$) is found to be the point at which the component of the flow normal to the ship track changes sign. In a uniformly rotating flow, the vorticity Ω of the eddy core is given by the slope of the normal velocity plotted against the distance ℓ along the track. Finally, the longitudinal velocity will be a constant along the ship track and can be used to estimate the distance of closest approach to the eddy, r_0. Given this information, an estimate of the eddy center location and core vorticity is obtained for each ADCP depth bin.

To illustrate the method, Figure 3b shows shipboard ADCP measurements taken over a three-hour period on 5 June 2015 as the ship passed the center of the large northern eddy (Murphy) on an almost straight trajectory (variations in the ship heading were less than 0.5 degrees during this time). Figure 3c shows the normal and longitudinal velocity components measured with respect to the ship track. The linear least-squares fit of the normal velocity component is shown in blue with a 95% confidence interval ($R^2 = 0.970$) and indicates a clear sign-change. The *x*-intercept of the linear fit is the estimated longitudinal position of the point of closest approach (vertical dashed line). In Figure 3c, the abscissa has been translated by this amount so that the sign-change occurs at $\ell = 0$.

The slope of the fit gives an estimate of the core cyclonic vorticity $\Omega = -1.9 \times 10^{-5}\ \mathrm{s}^{-1}$, corresponding to a rotational period of 3.9 days. This is somewhat faster than the vorticity estimated by fitting tangential velocities to a uniform vorticity profile (Figure 2b), which yields $\Omega = -1.6 \times 10^{-5}\ \mathrm{s}^{-1}$ and a rotational period of 4.4 days. We suspect that this is due to differential rotation across the eddy with slower tangential velocities at the eddy edge, especially on the southern flank

(discussed below). In such a case, fitting all measured ADCP velocities to a uniform vorticity profile would tend to underestimate the vorticity of the eddy core.

The longitudinal velocity component is nearly constant with speed 0.30 ms^{-1}, implying that the distance of closest approach to the eddy center was approximately 16.4 km. Figure 3b shows the eddy center position from the estimated distance of closest approach and the longitudinal position of the sign-change in V_N. The shaded region indicates the 95% confidence interval inferred from the uncertainties in these estimates.

3.3 Drifters

After the eddy centers were estimated, drifters were deployed at 3 sites along the S - N transect through the center of both the eddies (Table 2). The drifters were deployed a nominal distance of 4 km north and south of center in Freddy and 15 km (23 km) north (south) of center in Murphy. The remaining four drifters were deployed in other features of interest (Sup. Mat. Table S1). Drifters 1,2,3 and 4,5,6 were deployed across the core of Murphy and Freddy respectively (Figure 1a). Drifter positions and simultaneous SST fields were examined (where available) to confirm the drifters were inside Murphy or Freddy and that looping trajectories were most likely caused by eddy entrapment rather than by inertial oscillations. Only one of the drifters released in Murphy (D1, Table 2, Figure 4b) remained inside the eddy to complete more than one loop (i.e. completing 7 loops, Figure 4b). The positions of this drifter revealed that Murphy lasted at least 21 days post drifter deployment. In contrast, two of the drifters released in Freddy completed 3 loops (D4 and D6, Table 2, Figure 4f,h) and the third drifter completed 11 loops (D5, Table 2, Figure 4g). The drifter trajectories revealed that Freddy prevailed a minimum of 21 days. While inside the eddies the drifter trajectories from D1 and D5 (Figure 4b,g) showed the eddies moved straight-line distances (between the first and last drifter positions inside the eddies) of over 151 and 360 km for Murphy (9 days) and Freddy (21 days) respectively.

4 Physical Characteristics of the Eddies

4.1 Physical Characteristics

The broad range of observations collected during the field campaign allows us to comprehensively describe the physical characteristics of both the eddies, including their size, depth, rotation, speed and the time frames and location from birth to decay (Table 3). For example, we estimated the mean surface diameter of both the eddies using a range of different observations including; SST, S-ADCP, Triaxus, and where possible SSH. Each of these datasets required a degree of estimation. For example with the S-ADCP data there is a clear region of solid body rotation inside the eddy, a transition region towards the northern edge of the eddy where the EAC and the eddy core waters mix, and a region beyond the eddy where the EAC dominates and the eddy is no longer distinguishable. However, the good agreement between the different observations gives confidence in the results. In the case of Murphy, diameter estimates include 156 km (S-ADCP), 160 km

(Triaxus), 163 km SST and ~170 km from SSH. Thus we estimate the mean diameter to be 160 km on the day of sampling. In contrast for Freddy surface diameter estimates range 19 - 44 km from S-ADCP and 35 km from both SST and Triaxus. Our estimates of radius to maximum velocity using the eddy detection algorithm give 15 – 18 km radius, thus we therefore suggest a mean diameter at the surface of ~30 - 35 km.

Regarding the vertical extent of the eddies, the S-ADCP, with a range of ~820 m below the surface (OS75) revealed that both eddies extended at least to 820 m depth (Figure 5a). The ADCP transect suggests both eddies are tilting as evidenced by the lean in the zero velocity contour. Data from an LADCP attached to the CTD rosette (max range ~1000 m) shows that Murphy exceeds 1000 m depth, while it appears the vertical extent of Freddy is ~ 1000 m (Sup. Mat. Figures S2 and S3). It is remarkable that, although Freddy is just 1/4 the diameter of Murphy (35 km compared to 160 km), both eddies extend to more than 1000 m depth. Interestingly on the second visit to Freddy on 16 June (7 days later) the eddy appears to extend deeper, i.e. greater than 1000 m, (see Sup. Mat. Figure S4).

4.2 Hydrographic Properties

Vertical CTD profiles taken along transects through both eddies (Figure 6, Sup. Mat. Figures S5 and S6) to a maximum depth of 1000 m show the depth structure of their hydrographic properties. Temperature ranges ~5 - 23^{o}C in Murphy (~5 - 22^{o}C in Freddy) and practical salinity ranges 34.45 - 35.65 in both eddies. The surface waters of Murphy (top 150 m) consist of entirely Subtropical Lower Water (Condie and Dunn 2006), characterized by temperatures of 20 - 25^{o}C and Salinity of 35.5 - 35.7. Interestingly however the surface waters in Freddy (top 150 m) are made up of two different water masses. The waters in the core of Freddy are Central Tasman Water (Pearce 1981), with temperature of 15 - 20^{o}C, and salinity 35.5 - 35.65, likely derived from the shelf. However, around the edges of Freddy the waters are Subtropical Lower Water, identified by the warmer surface waters around the edges of the eddy (CTD casts 23 and 26), derived from the EAC.

The uplift of the isotachs is clearly evident across both eddies in all the CTD property transects (Figure 6, see also Supp. Mat Figures S5 and S6). In Murphy, the 17^{o}C isotherm is uplifted from ~225 m to 160 m (45 m total) over 75 km (0.6 m per km), whereas in Freddy the same isotherm is uplifted from 210 m to 125 m (85 m total) over just 25 km, i.e. 3.5 m per km (Figure 6). Interestingly, the point of maximum uplift of the isotachs (particularly evident in both salinity and temperature) is at the second cast (from the left, cast 24) above 400 m, and at the third cast (from the left, cast 22) below 450 m deep. This is further evidence that the core of the eddy is tilting to the west (and south) of the transect. This is discussed in more detail below. Spice (Figure 6) shows warm salty water wrapping around the edges of both the eddies associated with the warmer EAC waters flowing around the NE quadrant of the eddies. Tilting is most evident in the spice contours as the EAC waters 'lean' on the northeastern quadrant of both eddies.

The CTD profiles confirm that both the eddies extend to more than 1000 m depth (the limit of our CTD profiles), exemplified by the uplift of the 5^{o}C isotherm at 1000 m depth (Figure 6 top). As the

uplift at 1000 m is greater in Murphy than Freddy, we suspect that Freddy does not extend substantially further than 1000 m, however Murphy may extend a few hundred meters deeper than 1000 m.

Steric height anomalies across the eddies were calculated using both the Triaxus data (Figure 5c) using a level of no motion at 140 m, and the CTD data using a level of no motion at 980 m (Sup. Mat. Figure S7). In Murphy, the steric height ranges 0.18 m (1.53 - 1.71 m) from the core to the NE edge within EAC waters, whereas in Freddy the range is 0.22 m (1.47 - 1.69 m) referenced to a depth of 980 m. Remarkably, both eddies have similar steric height differences across their core (~0.06 m referenced to 140 m depth, ~0.20 m referenced to 980 m). This is compared to a range of 0.4 m (0.23 m) as derived from the Altika observations. The satellite estimates show a greater anomaly in Murphy suggesting we have not reached the bottom of the eddy with our estimates referenced to 980 m. However, when referenced to the same level (980 m), we were surprised to see that the small, young frontal eddy, which formed in < 200 m of water only 7 days prior has a similar steric height anomaly as the larger eddy Murphy. (See section 6.5.1 for more information on formation).

Using both the CTD/ LADCP data and the high-density hydrographic data from the Triaxus we calculated the Brunt-Väisälä frequency squared (N^2, Figure 5d) and Richardson number (not shown). N^2 shows that the thermocline and stratification is more pronounced in the larger older Murphy at 80 - 100 m depth. The vertical shear in the horizontal velocities in both eddies was strong enough to indicate unstable Richardson Numbers, Ri< 0.25. The Richardson number shows strongest shear instabilities overlying the thermocline in Murphy, co-located with high values of N^2, associated with strong lateral salinity intrusions (Figure 5 b). These instabilities are less apparent in Freddy.

T/S diagrams (Figure 7) from the CTD profiles taken through Freddy show the different water masses and the mixing that is occurring around the edges of the eddy as the shelf water (at the core) mixes with EAC waters (around the edges). The figure shows potential temperature and practical salinity for cast 20 (core of Freddy), cast 23 (southern edge of Freddy) and cast 26 (northern edge of Freddy) for the top 250 m of the water column. Interestingly, the core consists entirely of Central Tasman Water at the surface (top 250 m). The northern edge of the eddy which was impacted most by the EAC at the time the casts were taken is almost entirely EAC waters (Subtropical Lower Waters), with a surface temperature of nearly 1.5^{o}C warmer than the core. At the southern edge of the eddy there is EAC water below 120 m and central Tasman water above this depth. Below 250 m the T/S diagram follows a tighter curve. Oxygen and Fluorescence concentrations are both highest in the core of the eddy (cast 20) and lowest in the EAC water (cast 26) with the cast at the southern edge of the eddy again showing a mix between the two water masses.

Interestingly CTD casts 25 and 26 (in the northern quadrant of the Freddy) and to a lesser extent casts 34 and 35 (in the northwest quadrant of Freddy on the second visit, not shown) show clear evidence of water mass interleaving and mixing as the Subtropical Lower Water (EAC water) at the edges mixes with the Central Tasman Water inside the eddy. This is exemplified by a number of steps in the T/S curve in depths of 140 – 200 m as the EAC waters erode the edge of the eddy. These

layered lateral intrusions at the interface between predominantly EAC waters at the eddy edge, and predominantly Tasman Sea /shelf waters in the eddy core, are likely sites of enhanced lateral and vertical mixing. In contrast, while the surface waters of Murphy follow a tighter T/S curve suggesting the eddy formed from a single surface water mass, there is strong evidence of lateral salinity intrusions into the cooler core.

4.3 Biogeochemical Characteristics

Data from CTD transects (Figures 6 and 8) and Triaxus lines (Figures 5) are used to understand the vertical structure of the biogeochemical properties of the eddies. The high resolution Triaxus data shows the mixed layer depths (MLD) range 55 m (50 m) in the core, 60 - 80 m (85 m) on the coastal side and 85 m (80 – 100 m) on the EAC side in Murphy and Freddy respectively (Figure 5).

Nutrient profiles from the CTD casts show uplift in the core of both eddies (Figure 8, top row). Nitrate concentrations range from 0 at the surface to greater than 15 μmL^{-1} at ~350 m in Murphy, with uplift of nitrate near the center of the eddy of more than 100 m. Concentrations in Freddy are more uniformly associated with isotherms and are marginally lower than Murphy. For example the maximum nitrate concentration in the upper 400 m of Murphy is 14.6 μmL^{-1} (cast 12, 340 m) and 12.3 μmL^{-1} for Freddy (cast 24, 300 m). Asymmetry in the nutrient profiles is clearly evident in Freddy with uplifted concentrations in the southern quadrant (left side of transect) compared to the northern quadrant (right side of transect), which is under the influence of the EAC. Nitrate, phosphate and silicate follow similar patterns. This is consistent with the eddy tilt identified above, and discussed in detail below. Ammonia concentrations on the other hand (Figure 8 bottom row) are highest in the EAC waters around the edges of both the eddies. It is likely that the lower concentrations of nitrate, phosphate and silicate at the core of the eddy are indicative of uptake by phytoplankton.

Surface chl. *a* concentrations (Figures 5e, 6b, 8) are high in the surface mixed layer of both eddies, increasing towards the core; however concentrations are greater in Freddy (0.9 - 1.1 mgm^{-3}) than Murphy (0.8 - 0.9 mgm^{-3}). This is particularly evident in the high resolution surface Triaxus data (Figure 5). Dissolved oxygen patterns show high concentrations in the surface mixed layer and a subsurface minimum in both eddies (Figure 6c). The large northern eddy (Murphy) is characterized by a sharp vertical gradient in oxygen corresponding with the pronounced stratification (see N^2 in Figure 5d). In the frontal eddy however, DO and chl. *a* show a stronger relationship in the top 100 m (Figure 7). This might be indicative of a recent increase of the autotroph community in response to a source (uplift) of nitrates to the euphotic zone, consequentially leading to a net biological production of oxygen in Freddy's upper layers.

5 Dynamical Characteristics of the Eddies

5.1 Translational and Rotational Velocities and Eddy Nonlinearity

Sequential eddy center estimates using the method of closest approach (Table 4) were used to calculate the translational velocities of both eddies. Two estimates of the eddy center of Murphy (at 03:30 and 16:00 on 5 June) showed that the eddy center had shifted by 23 km in 12.5 hours in a direction 15.7°S of W, implying a translational velocity of approximately 0.5 ms^{-1} (Figure 9a). By contrast, the much smaller Freddy was more extensively sampled over a similar time period (00:15 on 9 June to 02:45 on 10 June), with seven eddy center estimates over 26.5 hours. The resulting translational velocity estimate was approximately 0.18 ms^{-1} in a direction 62.8°S of E (Figure 9b). However, Freddy's translational velocity varied between 0.08 - 0.31 ms^{-1} and changed direction from NNE to SW. A second visit to Freddy ~7 days later (16 June) found that the eddy center had translated by 106 km, implying a translational velocity of 0.19 ms^{-1} over that time period (Figure 9b).

The GPS-tracked drifters provided an independent estimate of translational velocities. The drifter positions were used to identify loops, most likely induced by spinning inside the eddy, where they were released (Figure 4). The distance and time between the positions of the drifters at the beginning and end of a loop were used to compute a translational velocity. Two of the drifters released to tag Murphy completed only one loop; a third drifter completed seven loops, yielding a mean translational velocity and standard deviation (across loops by all drifters) of 0.12 ± 0.05 ms^{-1}, somewhat slower than that inferred from the eddy center estimates. Three drifters remained inside Freddy and completed 3, 3, and 11 loops, respectively; we found a mean translational velocity across loops by all drifters of 0.15 ± 0.08 ms^{-1}, which is consistent with that obtained from the eddy center estimates. Although the mean translational velocities are of similar order of magnitude, the size of Freddy is 3 - 4 times smaller than that of Murphy implying a longer navigational time between sampling stations to remain inside Murphy. Adjacent drifter positions were used to compute the tangential velocities inside the eddies; we obtained a mean of 0.5 ± 0.15 ms^{-1} for Freddy and 0.5 ± 0.18 ms^{-1} for Murphy. Given Freddy and Murphy estimated radii (i.e. 15 and 80 km) these velocities imply 5.3×10^{-6} and 9.9×10^{-7} rotations per second (or 2.18 and 11.7 days for a full rotation) respectively at the edge of the eddy. However, the drifters were not necessarily at the eddy edge or following circular trajectories, thus the time for drifters to complete loops varied largely (15 hours – 4 days in Freddy, and 2-8 days in Murphy). Although these are not expected to match rotational estimates from ADCP data they have a similar order of magnitude.

The degree to which an eddy can trap fluid within its core depends on the nonlinearity of the eddy. A useful measure of eddy nonlinearity is U/c, where U is the rotational velocity of the eddy and c is the translational velocity. For values of $U/c > 1$, transforming coordinates to a frame that is co-moving with the eddy results in closed streamlines that trap fluid and biological characteristics within the core of the eddy (e.g. Early et al., 2011). By contrast, when $U/c < 1$, the feature can be considered as a linear wave that does not trap fluid parcels as it propagates. In their survey of 16 years of altimetric observations, Chelton et al. (2011) used U/c to quantify the nonlinearity of mesoscale ocean eddies and found qualitatively similar results compared to other commonly used eddy nonlinearity metrics.

Klocker et al. (2016) used a similar nonlinearity parameter to distinguish linear and nonlinear regimes of ocean eddies. Although both of these studies focused on mesoscale features identified using satellite altimetry, the nonlinearity parameter U/c is equally valid on the scales of the eddies considered here.

Using the mean translational and rotational velocities estimated from the GPS-tracked drifter trajectories, we find values of U/c ~4.2 ± 2.5 for Murphy and ~3.3 ± 2.8 for Freddy. Freddy had a slightly smaller value for the nonlinearity parameter because of its higher mean translational speed. These values suggest that both Murphy and Freddy were significantly nonlinear and were capable of trapping fluid within their cores. This is also strongly suggested by the fact that several of the drifters remained within both eddies for times similar to or larger than the rotation periods: 4.9, 8.4 and 21.2 days for Murphy, and 3.3, 3.4, and 21.3 days for Freddy respectively (Figure 4).

5.2 Eddy Tilt

Eddy tilt was calculated from the change in the estimated eddy center position with depth. The zonal and meridional displacements of the center of the two eddies are shown as functions of depth in Figure 10a-d. To estimate the tilt of the eddy in the upper water column, a least-squares fit was performed for the location of the eddy center in both the zonal and meridional directions, weighted by the inverse error variance in the eddy center estimate at each depth. For both eddies the observed center displacement with depth is well described by a linear tilt ($R^2 \sim 0.86 - 0.98$) except at the surface (~50 m) where surface dynamics are expected to play a dominant role.

For Murphy, the resulting tilt is equivalent to 3.3 km for every 100 m of depth in a direction 21.2°S of W, approximately onto the continental slope. This is a significant tilt, equivalent to 23 km over 700 m (the observational range of the OS75kHz ADCP sensor was 820 m). Freddy had a tilt of 1.5 km for every 100 m of depth, directed 19.7°S of W, also onto the continental shelf. This translates into 10 km lateral displacement over the upper 700 m of the water column. Again, this is a significant tilt, especially when compared with the ~30 - 35 km diameter of Freddy.

We visited Freddy a second time on 16 June (Sup. Mat. Figure S8). However, by this stage the OS75kHz ADCP (~820 m range) had failed, thus we were limited to the OS150kHz with a range of ~ 330 m. Despite this limitation, we estimated the tilt in the top 330 m in the same manner. Results (Sup. Mat. Figure S9) show a tilt of 2.8 km per 100 m of depth in a direction 64.4°S of E, that is, no longer onto the continental slope.

5.3 Ageostrophy

The estimated rotational period $T = 2\pi/|\Omega|$ and Rossby number, $\mathrm{Ro} = |\Omega|/|f|$, as functions of depth for the cores of the two eddies are shown in Figure 11, where Ω is the estimated eddy core vorticity and f is the Coriolis parameter at the eddy center. For Murphy, the rotation period varies between 3.8±0.5 days (Ro = 0.29±0.04) near the surface and 5.3±1.1 days (Ro = 0.20±0.04) at 600 m, indicating that the eddy is predominantly in geostrophic balance ($\mathrm{Ro} \ll 1$). By contrast, Freddy

has a rotation period of 1.4±0.1 days (Ro = 0.64±0.03) near the surface, while at 600 m the rotation period is approximately 3.4±0.9 days (Ro = 0.27±0.07). Uncertainties in the rotation period and Rossby number are based on the 95% confidence intervals indicated in Figure 11 and are estimated from the least-squares fitting procedure used in the method of closest approach (Section 3.2). The estimated Rossby numbers are typical for frontal eddies observed in high-frequency surface current measurements in this region (Schaeffer et al., *Submitted*).

The largest observed Rossby numbers (0.5-0.65) are in the upper 250 m of Freddy where rotation rates (1-2 days) are fastest. Rossby numbers with magnitude not much smaller than one indicate the existence of a significant ageostrophic component to the flow, such as nonlinear advection or centripetal acceleration. It is important to note that ageostrophic flow can still be balanced and is not necessarily indicative of the presence of submesoscale processes (Capet et al. 2008). Flows in which the horizontal pressure gradient is balanced by centripetal acceleration, rather than the Coriolis force, are said to be in cyclostrophic balance, while flows in which both the Coriolis force and centripetal acceleration balance the horizontal pressure gradient are in gradient-wind balance (McWilliams 1985). For example, Brannigan et al. (2015) showed that the degree of geostrophic balance in a numerical simulation of mid-latitude open ocean turbulence decreases as the resolution is increased to permit submesoscale dynamics; however, unbalanced submesoscale motions constituted a small portion of the flow compared with the balanced components, including cyclostrophic balance.

An estimate of the geostrophic and ageostrophic components of the eddy flow field was provided by serendipitous along-track altimetric measurements across both eddies by the AltiKa altimeter carried aboard the SARAL satellite. The satellite passed almost directly over the eddy center at nearly the same time as the in-situ sampling (Figure 9a, b; green dots). The measured along-track sea-level anomaly (SLA) was compared with the SLA of an idealized eddy flow field with a Gaussian profile of the form

$$V(R) = \Omega L e^{-R^2/2L_e^2}$$

where R is the distance from the eddy center, L_e is the estimated e-folding length scale of the eddy core, and Ω is the vorticity of the eddy core at the surface. The parameters L_e and Ω were estimated from shipboard ADCP measurements as $L_e \approx 80$ km, $\Omega \approx -1.14 \times 10^{-5}$ s^{-1} for Murphy and $L_e \approx 25$ km, $\Omega \approx -4.51 \times 10^{-5}$ s^{-1} for Freddy. If the satellite ground track passes the eddy center at a distance of R_0 then $R = (l^2 + R_0^2)^{1/2}$, where l is the distance along the ground track (Figure 12a). For Murphy, the distance of closest approach was negligible ($R_0 \approx 0$ km) but for Freddy we estimated $R_0 \approx 20$ km. (Note that these parameters were chosen to match the observations as closely as possible, but our results are not sensitive to the exact values used.)

The Gaussian flow profile will have both Coriolis (geostrophic) and centripetal (cyclostrophic) SLA components given by

$$SLA_{Coriolis} = g^{-1} \int fv\, dl, \quad SLA_{Centripetal} = g^{-1} \int \frac{V^2}{R} dl$$

The observed AltiKa SLA (detrended) and the estimated SLA contributions from the Coriolis and centripetal components of the idealized Gaussian flow field for each eddy are shown as functions of the along-track distance in Figures 12b,c. Also shown is the total SLA (the sum of the Coriolis and centripetal components). Both eddies have similar maximum SLA at the core of approximately 0.3 - 0.45 m, but of course the core of Freddy is much more compact than that of Murphy. Notice that the SLA of Murphy is fairly well approximated by a Gaussian profile while Freddy's SLA profile is more acute. This is due to the fact that the satellite passed directly over the center of Murphy but not of Freddy. (Note that the satellite overpasses and eddy center estimates indicated in Figure 9 are from slightly different times; see caption for details). In the case of Freddy, this slight offset meant that the Gaussian profile becomes more pointed when projected in the along-track coordinate.

In the case of both Murphy and Freddy, the total SLA is dominated by the contribution from the Coriolis term, indicating that both of these eddies are primarily in geostrophic balance. However, as a percentage of the total SLA at the point of closest approach, the centripetal term makes a larger contribution to Freddy (~20%) than it does for Murphy (~9%). It is possible that, had SARAL passed directly over the center of Freddy, the estimated contribution of the centripetal term to the total SLA at the eddy center would be even higher. Nonetheless, it is clear that the ageostrophic (centripetal) component of Freddy was at least twice that of Murphy.

When we visited Freddy the second time (16 June), we found that the rotation rates ranged from 2.1 - 4.1 days from the surface to 330 m, with Rossby numbers ranging 0.43 - 0.22 (surface to 330 m), indicating that the eddy was primarily in geostrophic balance (Sup. Mat. Figure S10). The eddy appeared to extend more deeply (Sup. Mat. Figure S4), but we were unable to estimate the rotation rates below 330 m due to equipment failure. Unfortunately, altimetric measurements of SLA across Freddy were not available during the second sampling period.

5.4 Differential Rotation

The vorticities and rotational periods estimated using the method of closest approach correspond to the rotation of the eddy core. If the eddy is under the influence of a torque, for example from wind forcing, interactions with the ocean floor, or adjacent currents, then the rotational speed of the eddy may change both from the center to the edge of the eddy, and in different quadrants of the eddy. Differential rotation may also arise if the eddy is elliptical. To study this, tangential velocities were calculated from the ADCP velocity measurements across both eddies, from the center to the edge and in all quadrants. Figure 13 plots these tangential velocities against the tangential velocity that would be *expected* given a uniformly rotating flow with the same vorticity as the eddy core, i.e. $V_T = \Omega r$. The diagonal line separates regions where the measured tangential velocities are faster or slower than expected from uniform rotation, while points below the horizontal line at $V_T = 0$ show tangential velocities that are in the opposite direction to the rotation of the eddy core, that is, anti-cyclonic rotation.

The color scale indicates different sectors of the eddy, so that blue dots correspond to measurements taken on the northern side of the eddy, while red dots are from the southern side, and so on. In the

case of Murphy, there are a few locations that rotate at or above the vorticity in the eddy core, notably the northern and northwestern flank. This is where the eddy meets and is sheared by the EAC, which flows eastward on the northern flank of the eddy. The warmer waters of the EAC are clearly visible in Figure 9a. The fastest measured tangential velocities (~1 ms^{-1}) are actually from deep inside the EAC. By comparison, the other quadrants of the eddy tend to rotate more slowly than the eddy core, particularly the southern quadrant.

A similar analysis carried out for the smaller Freddy shows a larger spread of tangential velocities both faster and slower than rotation of the eddy core (Figure 13b). The southern flank rotates more slowly, especially where it begins to interact with the east-west thermal front dividing the warmer waters from a cold watermass associated with a large cyclonic eddy to the south (Figure 9b). The fastest measured velocities (~1 ms^{-1}) are on the northern and eastern flanks of the eddy where the EAC flows past in an E-SE direction. The fact that the NE edge of the eddy is rotating considerably faster than the eddy core suggests that the EAC is transferring angular momentum to the eddy, possibly maintaining it against the tendency to dissipate or slow down as it moves into deeper water.

6 Discussion

6.1 The 3-D Structure of the Eddies

Accurate vertical structures of mesoscale eddies are often observationally inaccessible (Zhang et al. 2014). Here we have clearly observed the three dimensional structure of two contrasting cyclonic eddies; Murphy, a large mesoscale eddy, and Freddy, a smaller frontal eddy. Several studies, including Zhang et al. (2014) and Rykova and Oke (2015), have attempted to identify the 3-D structure of 'mean' mesoscale cyclonic and anti-cyclonic eddies using Argo float and remote sensed data. Rykova and Oke (2015) show the classic view of a mesoscale cyclonic eddy in solid body rotation with symmetric isopycnal uplift in the core of the eddy. They identified salinity (temperature) anomalies persisting to depths of 1000 m (2000 m), respectively. Our results show that Murphy penetrated to more than 1000 m whereas Freddy was approximately 1000 m deep (based on both ADCP and hydrographic observations). This is in contrast to the modeling study of Oke and Griffin (2011), who identified a mesoscale cyclonic eddy of similar size (100 km diameter) extending the full depth of the water column (~4000 m) in this region. Observations are scarce at such depths, but our results (and those of Rykova and Oke 2015) suggest that it is likely that models can over-represent the vertical extent of the eddies. Overestimating eddy structures will impact on the calculations of heat content carried by eddies, which is important to get right in this region of rapid ocean warming.

Notably, our results show significant tilting of both the eddy cores through the water column, irrespective of the geostrophy or vorticity in the eddies. This is associated with asymmetric uplift through the core of both the eddies. Both eddies were tilting towards the SW onto the continental slope, which is also diagonally away from the rotational lever provided by the EAC flowing along the NE quadrant of the eddies. For Murphy (Freddy), the tilt is equivalent to 23 km (10 km) lateral displacement over the upper 700 m of the water column. In their modeling study, Oke and Griffin

(2011) also identified eddy tilting, toward the continental slope. Their results showed a mean tilt of 28 km over 4.5 km depth, which is far less than the tilts observed in Freddy and Murphy. However, their results also showed that the tilt is surface intensified (i.e. not linear throughout the full water column) and that their particular mesoscale eddy had a time averaged tilt of 20 km over the top 2 km of the water column and an instantaneous maximum tilt of up to 50 km in the top 1km. This shows that tilting is a significant process occurring in both mesoscale and frontal eddies and thus requires further investigation to understand the mechanism driving it, and the impact on biological production.

6.2 Impact of differential rotation rates

Using the S-ADCP velocity data we were able to calculate rotation rates around the eddies and identify regions that were rotating faster or slower than expected from uniform rotation. The observation of differential rotation rates is in agreement with the results of Schaeffer et al. (Sub) who surveyed frontal eddies over a 12 month period to the north of this domain. Using HF radar observations of surface velocities they showed that frontal eddies intensified horizontal divergence at the leading edge (downstream of the eddy) and convergence on its trailing edge (upstream), what we are referring to here as the SW and NE quadrants respectively. In the case of the two eddies presented here, the region of convergence corresponds with the NE quadrant where the EAC drives the eddy, exemplified in our data by rotational speeds greater than at the core, whereas the region of divergence (in the southern or leading quadrant) is exemplified by rotational speeds slower than at the core (Figure 13). This asymmetry is expected to drive upward and downward vertical velocities and explains why the MLD is deeper on the EAC edge (convergence and downwelling) than on the coastal edge (divergence and upwelling). This positive-negative signature of upwelling and downwelling has also been observed and modeled in the Gulf Stream (Gula et al. 2016).

6.3 The Lifespan of the Eddies

Due to the small size of Freddy, satellite imagery alone is insufficient for tracking the lifespan of the eddy. While the eddy is visible at times in MODIS Aqua SST data, the data is often contaminated by cloud cover. Using SST alone, one would be misled to believe that the lifespan of Freddy was ~ 10 days (June 2 - 13), however this is because there are no further clear images until June 23 when the eddy is no longer visible. For this reason, drifters are the most suitable option for tracking the eddy remotely. Using the drifters as a positioning system, we were able to return to Freddy a second time on June 16 (despite the lack of satellite imagery) and the current velocities confirmed the presence of the eddy. Drifters however are not totally reliable either: two of our drifters were expelled from both eddies after only 3 days (Figure 4). From the drifter that remained in Freddy, we estimate the eddy persisted for at least 21 days after the drifter was deployed (until June 30), giving a lifespan of ~28 days. The next clear SST image after this time was on 1 July, which showed that Freddy either no longer existed or no longer had a surface signature (Sup. Mat. Figure S1).

Detecting the decay of a mesoscale eddy can be more straightforward. However one needs to be mindful that the detection of mesoscale eddies in gridded maps of altimetric sea level depends on their location with respect to the ground tracks of the satellites, so small eddies can spuriously

disappear. Satellite imagery of SST and SSH show that Murphy persisted 43 and 42 days respectively (not shown), while one drifter appeared to remain in a cyclonic eddy until June 26 (Figure 4), indicating a lifespan of 47 days (Table 3). Interestingly this is shorter than the maximum lifespan for a mesoscale cyclonic eddy in the region (~150 days, Cetina Heredia et al. Pers. Comm.).

A ROMS modeling study by Macdonald et al. (2016) investigated the formation of a cyclonic eddy in the region. Their results showed that the CCE formed through the transfer of mean kinetic energy to eddy kinetic energy. This occurred in a region of high strain and large vorticity gradient between the continental shelf waters and the fast flowing EAC. Thus we suspect that both our eddies are fed by the spin of the WBC across their NE quadrants which contributes to both sustaining the eddies and causes the asymmetric tilt of the eddies. Furthermore in the case of the smaller Freddy the EAC contributes to the surface intensified ageostrophy. This is the subject of further work.

Our observational data showed that Murphy was able to grow to become a large mesoscale eddy (~160 km in diameter at time of sampling), lasting 43 - 47 days (Table 3), whereas Freddy remained small for its duration (~19 - 44 km diameter at time of sampling), lasting ~28 days (Table 3). We do not yet know the mechanism that caused the eddies to decay, or why Murphy lasted significantly longer than Freddy. However, in the case of the frontal eddy modeled by Macdonald et al. (2016) that grew to a diameter of over 100 km and lasted more than 20 days, the eddy formed in a region of high velocity shear between shelf and EAC waters. They showed that the eddy entrained negative vorticity shelf waters at the core as it grew. They showed that it was a transfer of kinetic energy from the EAC that sustained the eddy and entrainment of shelf waters that allowed it to grow.
In the Gulf Stream region, where frontal eddies appear to remain topographically trapped along the front of the WBC (with formation occurring off Miami (~26 - 30^{o}N) and decay between 33 - 36^{o}N approaching the Charleston bump (Lee et al. 1991 and Gula et al. 2016)), the Charleston bump itself has been suggested as a contributor to eddy decay. Further work is required to understand the mechanism behind growth and decay of eddies in the EAC region.

6.4 Statistical Representativeness

Understanding the statistical representativeness of our results helps to put them in the context of the overall productivity of the EAC System. From particle tracking simulations run with velocity fields from the Ocean Forecast for the Earth Simulator (OFES), Cetina-Heredia et al. (Pers. Comm.) found that mesoscale anti-cyclonic (cyclonic) eddies in the Tasman Sea region have diameters between 33 - 280 km (30 - 256 km), with mean diameters of 127 and 113 km for anti-cyclones and cyclones respectively. In addition, they have maximum lifespans of ~230 (~150) days respectively, and rotational speeds between of 0.01 - 1.2 ms^{-1} with a mean of 0.38 ms^{-1}. Our results showed that Murphy (diameter ~ 160 km) is within the size range identified for OFES eddies, and by Everett et al. (2012), with diameters of <100-300 km, with a mean diameter of 164 km. Everett et al. (2012) showed that eddies in the Tasman Sea have typical rotation speeds of ~0.23 ms^{-1} and on any given day there are between 16-18 cyclonic and anti-cyclonic eddies in the region. Thus, the observed Eddy Murphy is typical of mesoscale cyclones found in the EAC system.

Observational studies of small (frontal) eddies such as Freddy are the subject of very recent work and have not been conducted basin wide or globally due to a lack of high resolution observations. In this region, however, high-resolution (~1.5 km) surface current velocities from HF radar observations over an approximately 100 km square region off Coffs Harbour (~30^{o}S) are revealing the persistent evolution of submesoscale frontal eddies and their poleward propagation associated with meanders of the EAC (Schaeffer et al. Sub.). These cyclonic structures with diameter of 10 - 60 km are typically advected poleward, along the inshore edge of the EAC, with translational velocities of 0.3-0.4 ms^{-1} or 27 - 36 km per day, (Schaeffer et al. Sub.). Based on the intermittent satellite and radar pictures preceding Freddy's sampling, we suggest that Freddy originated as a small billow that grew to form a cyclonic eddy on the shelf that was advected offshore with the EAC as it separated from the coast. The reduced advection speed of the small eddy (0.15 ms^{-1} at the time it was sampled) is probably a result of the deeper topography after the eddy left the shelf and lower volume transport of the eastward component of the EAC (James et al., 1999). Cyclonic features similar to Freddy have been observed at 30^{o}S under the HF radar footprint (upstream of where we sampled Freddy) every few weeks, all year long (Schaeffer et al. Sub.). In addition, frontal eddies have often been observed in satellite imagery of SST and ocean color.

It is also important to relate our chl. *a* estimates to productivity in the EAC system more broadly. Using satellite remote sensed ocean color data to survey more than 2400 cyclonic eddies Everett et al. (2012) found a mean chl. *a* concentration of 0.3 - 0.38 mgm^{-3}. In contrast, they found the mean chl. *a* concentrations from more than 3000 anticyclonic eddies to be 0.17 - 0.25 mgm^{-3}. Figure 1c shows remote sensed surface chl. *a* concentrations of ~0.4 mgm^{-3} in Murphy and 0.7 - 0.8 mgm^{-3} in Freddy. Using the Triaxus data we estimated the chl. *a* concentrations in the surface mixed layer (~0 – 50 m) to be 0.6 (0.7 - 1.11 mgm^{-3}) in Murphy and Freddy respectively. Thus while the chl. *a* concentration in the surface waters of Murphy is characteristic of mesoscale cyclones within the EAC system, Freddy is significantly more productive than typical mesoscale cyclones. Although presently under-observed, we expect that frontal eddies such as Freddy make a significant contribution to the overall productivity in the region due to the regularity with which they are formed, and their propensity for higher chl. *a* concentrations.

6.5 Biological Implications

6.5.1 Entrainment of Shelf Waters

One of the core goals of the research cruise was to understand the role of frontal eddies as planktonic incubators, thus testing the model of Bakun's (1996, 2006) theory of productivity in eddies. Bakun (1996, 2006) identified a three-stage synthesis of favorable reproductive habitats in ocean eddies; i) enrichment such as upwelling, ii) concentration such as convergence and iii) retention; keeping larvae un-diluted and geographically isolated. Thus knowing how and when the two eddies formed is of significance, as we need to understand the composition of the source waters as the eddy grew. For example, if the eddy grew from shelf waters, potentially laden with nutrients and phytoplankton (e.g Armbrecht et al. 2014, 2015), eggs and seed populations of larval fish, (e.g. Mullaney and

Suthers 2013, Everett et al. 2015, Macdonald et al. 2016) the biological productivity of the eddy has potential to be significantly greater than if the eddy formed from oligotrophic EAC waters with the only source of nutrient from vertical pumping in the core of the eddy.

A numerical modeling investigation into a cyclonic eddy (diameter 60 – 120 km) that formed in the region showed that proximity to the shelf was essential for entrainment of shelf waters (Everett et al. 2015). Using a dye tracer Everett et al. (2015) showed that surface waters within the cyclonic eddy (top 50 m) were almost entirely of shelf origin. Using in-situ mooring data on the continental shelf at 30°S, Schaeffer et al. (2014) showed that onshore fluctuations in the EAC and encroachment of eddies on shelf (which occurred at periods of 90 - 100 days) can drive onshore bottom boundary layer transport across the shelf, bringing an injection of cold (nutrient-richer) bottom water. This cold bottom water may in turn be entrained into the frontal eddies that form adjacent to the jet, thereby increasing their productivity potential.

In the case of Eddy Murphy we used particle back tracking (using AVISO derived estimates of geostrophic velocities) overlaid on SST to estimate the timing and location of eddy formation (not shown). Results revealed that Murphy formed adjacent to the shelf at ~28°S on approximately the 9th of May primarily from offshore waters (as identified in the water mass analysis). However as the eddy was advected offshore along the EAC front, the particle tracking suggests that it entrained water from both the east and west as it grew.

SST imagery showed that Freddy formed from a billow on the continental shelf (at ~31.5°S, Sup. Mat. Figure S1) and was subsequently swept offshore along the frontal edge of the EAC. Water mass characteristics (Figure 7) showed that in the top 200 – 300 m the core of the eddy consisted of shelf waters, while the edges of the eddy were dominated by EAC waters, with significant mixing occurring in between. Within < 7 days of generation, Freddy had moved off the shelf into more than 4000 m of water, and had extended to more than 900 m below the surface, and was translated hundreds of kilometers offshore in a matter of weeks. Freddy received no further shelf waters after it moved offshore, and the deep waters of the eddy were primarily EAC waters. However, its generation on the shelf may have allowed sufficient seed populations to become entrained, thus the cyclonic eddy was able to support the production of coastal larval fish species (see section 6.5.3).

6.5.2 Eddy Tilting and Vertical Uplift

The hydrographic data show that the tilting we observed within both eddies is significant for the biogeochemical response in the eddies. The asymmetric upward (and downward) movement of the isopycnals that we identified results in asymmetric vertical excursions of nutrients and planktonic organisms as they rotate around the eddy. This results in organisms moving up and down, or into and out of the euphotic zone as they rotate around the eddy. This is exemplified by greater chl. *a* concentrations on the southern flanks of both eddies – higher in the water column. Similar vertical excursions were identified in a modeling study of a tilting cyclonic eddy (Everett et al. 2015, their Figure 8), who showed that modeled particles underwent vertical excursions of up to 250 m as they rotated around a cyclonic eddy.

As we do not have information on the temporal evolution of the eddies as they evolved, we are not able to estimate an upwelling rate. However Schaeffer et al. (Sub.) suggested vertical velocities O(10-100 m per day) in frontal eddies on the shelf in this region based on the uplift of isotherms associated with surface horizontal divergence. These uplift rates are typical of submesoscale motions, which can exceed 1mms^{-1} or 100 m per day (Mahadevan and Tandon 2006) and make a disproportionately large contribution to phytoplankton production in nutrient-limited region (Mahadevan 2016).

6.5.3 Frontal Eddies as Planktonic Incubators

Although frontal eddies are short lived (1 - 4 weeks) this time frame is consistent with the larval period of many coastal fish species (e.g. Syahailatua et al. 2011, Matis et al. 2014). An EAC frontal eddy was opportunistically sampled for biological productivity and larval fish composition and abundance in October 2006 revealing a distinctive community of fish larvae and zooplankton (Mullaney and Suthers 2013). Subsequently Matis et al. (2014) showed that recent proximity of a cyclonic eddy to the continental shelf may have contributed to an increase in the presence of coastal larval fish species through continental shelf entrainment, indicating a potential offshore nursery ground for coastal fish species.

We expect that the phytoplankton and larval fish composition of the two eddies will differ based on their formation location, the age of the water masses and potential for different seed populations. Multiple EZ net tows were undertaken at a range of depths, both inside and outside each of the eddies as well as on the shelf, to assess larval fish diversity, and abundance. Samples were sorted and abundances were estimated. Notably, Freddy showed relatively high concentrations of coastal species. For example, *Sparidae* (bream etc), *Platycephalidae* (flatheads), *Mullidae* (mullets), *Cheilodactylidae* (morwongs) were highest in abundance in the frontal eddy (Suthers Pers. Comm.), when compared both with shelf waters and the larger Murphy.

The high concentrations of larval fish species in the frontal eddy, which were even greater than the coastal concentrations, are an indication of the retentive nature of the eddy. It also suggests that Freddy is in fact acting as a planktonic incubator, growing coastal populations that were seeded at the coast and subsequently advected offshore. Significantly, the frequency and duration of these small eddies at 1 - 4 weeks is sufficient to complete the larval period for coastal larval fish (such as those mentioned above).

In the eddies studied here, the EAC flow is an order of magnitude greater than the poleward advection of the eddy. In addition, both the eddies are highly non-linear meaning the rotational velocity is greater than the translational velocity. Thus organisms such as plankton are retained in the eddy and are not swept hundreds of kilometers offshore away from coastal habitats. In addition, frontal eddies are often geographically retained near the shelf, providing the third and final stage of Bakun's (1996) synthesis. Importantly, the timescales associated with frontal eddies, including the

vertical transport of nutrients are similar to the timescales of phytoplankton growth and production. Thus frontal eddies are very effective in supporting local primary production.

7 Conclusions

We have presented a tale of two eddies: one a mesoscale cyclonic eddy typical of the EAC system, the other a smaller cyclonic frontal eddy. This study represents the first 3-D in-situ observations of a frontal eddy in the EAC System, employing a suite of shipboard observations (including towed body CTD profiles, ~1000 m CTD casts from a shipboard rosette mounted with L-ADCP, deep and shallow shipboard ADCP observations) combined with surface drifters and high-resolution satellite imagery from MODIS (SST and color), AVHRR (SST) and altimetry from the new SARAL/Altika mission. Using this comprehensive arsenal of observations we were able to diagnose the physical, hydrographic, biogeochemical, and dynamical characteristics of both eddies.

The smaller frontal eddy was ~35 km in diameter, lived ~ 30 days, and extended to a depth of at least 1000 m with a sea level anomaly of ~0.4 m. The frontal eddy exhibited high Rossby number, low Richardson number, and strong ageostrophy in the surface waters as well as differential rotation rates resulting from external torque being applied from the EAC as the eddy moved off the continental shelf where it was formed, into deeper waters. By contrast the mesoscale cyclonic eddy (Murphy) was representative of typical mesoscale eddies in diameter, depth and chlorophyll concentration, although with a lifespan of ~47 days it was shorter lived than most. Both eddies exhibited significant tilt through the water column, in addition, the mesoscale eddy although primarily geostrophic, exhibited evidence of submesoscale dynamics above the thermocline. Despite its small size, the frontal eddy was high in both nutrient and chlorophyll *a* concentrations and was able to sustain populations of shelf larval fish species.

Frontal eddies (some of which are submesoscale) form regularly along the inside edge of the EAC, and thus we conclude that they have a clear potential to contribute significantly to the overall productivity of the oligotrophic EAC System. We suggest that other such studies be undertaken in analogous WBC regions to determine the significance of frontal eddies to overall productivity. In addition, high resolution features such as frontal eddies are not yet resolved in global biogeochemical models, however our results imply that small frontal eddies play an important role in the large-scale distribution of tracers, and contribute to building ecosystem structure.

Acknowledgments and Data

We acknowledge the extraordinary effort of all the Australian Marine National Facility staff and the ship's crew who worked tirelessly during a difficult shakedown voyage of a new research vessel under the able guidance of the master M. Watson and the voyage managers D. Mackenzie and M. Macguire. We are grateful for the commitment and dedication of M. Reyner and his hydrochemistry team: C. Schwanger, and C. Rees, computing support from S. Wilde and H. Barker, mechanical and electronics support from B. Muir A. Tyndall and M. Lewis particularly with the towed body and nets, and swath support from D. Watts and M. Boyd. In addition we thank our fellow voyage participants who worked closely together to make the voyage both fun and successful. MODIS and

AVHRR satellite data was sourced as part of the Integrated Marine Observing System (IMOS) - IMOS is supported by the Australian Government through the National Collaborative Research Infrastructure Strategy and the Super Science Initiative. All data collected on the cruise, and from IMOS are available through the Australian Ocean Data Network www.aodn.org.au. The original altimeter products were produced by Ssalto/Duacs and distributed by AVISO, with support from CNES (http://www.aviso.altimetry.fr/duacs/). Altika data is sourced from the RADS database. Surface drifters were provided by R. Lumpkin and S. Dolk at the NOAA surface drifter program and data are available at (http://www.aoml.noaa.gov/phod/dac/gdp_information.php). MR and SK were partially supported by a UNSW Silverstar Research Grant. SK is also an Associate Investigator in the ARC Center for Excellence in Climate Systems Science, which is supported by the Australian Research Council via grant CE110001028. PCH and CR are partially supported by an Australian Research Council Linkage Project grant to MR (LP150100064). PCH's participation in the cruise was partially supported by the Australian Research Council (DE130101336). This is contribution number 190 from the Sydney Institute of Marine Science.

References

Armbrecht, L. H., Roughan, M., Rossi, V., Schaeffer, A., Davies, P. L., Waite, A. M. and Armand, L. K. (2014) Phytoplankton composition under contrasting oceanographic conditions in a biological hotspot: Solitary Islands Marine Park (Eastern Australia)' Continental Shelf Research 75, pages 54-67. doi:10.1016/j.csr.2013.11.024.

Armbrecht, L.H., Schaeffer, A., Roughan, M., Armand, L.K. (2015) Interactions between seasonality and oceanic forcing drive the phytoplankton variability in the tropical-temperate transition zone (~30°S) of Eastern Australia. J. Marine Systems 144, p 92-106 doi: 10.1016/j.jmarsys.2014.11.008

Bakun, A. (1996), Freddy Patterns in the Ocean: Ocean Processes and Marine Population Dynamics. Univ California. 323 pp.

Bakun A (2006), Fronts and eddies as key structures in the habitat of marine fish larvae: Opportunity, adaptive response and competitive advantage. Scientia Marina 70:105-122

Brannigan, L., Marshall, D.P., Naveira-Garabato, A. and Nurser, A.J.G. (2015). The seasonal cycle of submesoscale flows. Ocean Modelling 92: 69-84.

Benitez-Nelson, C. R., R. R. Bidigare, T.D. Dickey, M.R. Landry, C. L. Leonard, S. L. Brown, F. Nencioli, Y. M. R. Kanchan Maiti, J. W. Becker, T. S. Bibby, W. Black, W. Cai, C. A. Carlson, F. Chen, V. S. Kuwahara, C. Mahaffey, P. M. McAndrew, P. D. Quay, M. S. Rappé, K. E. Selph, M. P. Simmons, E. J. Yang (2007), Mesoscale Eddies Drive Increased Silica Export in the Subtropical Pacific Ocean. 316, 5827, 1017-102, doi: 10.1126/science.1136221

Bowen, M. M., J. L. Wilkin, and W. J. Emery (2005), Variability and forcing of the East Australian Current, J. Geophys. Res., 110, C03019, doi:10.1029/2004JC002533.

Capet, X., McWilliams, J.C., Molemaker, M.J. and Shchepetkin, A.F. (2008). Mesoscale to submesoscale transition in the California Current System. Part II: Frontal processes. J. Phys. Oceanogr. 38: 44-64.

Chelton, D. B., P. Gaube, M. G. Schlax, J. J. Early, R. M. Samelson (2011a). The Influence of Nonlinear Mesoscale Eddies on Near-Surface Oceanic Chlorophyll. Science 334, 328. doi:10.1126/science.1208897

Chelton, D. B., M. G. Schlax, R. M. Samelson (2011b), Global observations of nonlinear mesoscale eddies, Prog.

Oceanogr., 91 (2), 167-216, doi:10.1016/j.pocean.2011.01.002.

Cetina Heredia, P. M. Roughan E. Van Sebille, M.A. Coleman, (2014) 'Long-term trends in the East Australian Current separation latitude and eddy driven transport. J. Geophys. Res. Oceans, 119, doi:10.1002/2014JC010071.

Condie, S. A. and J. R. Dunn, (2006), Seasonal characteristics of the surface mixed layer in the Australasian region: implications for primary production regimes and biogeography. Marine and Freshwater Research, 2006, 57, 569–590

Cresswell, G. (1982), The coalescence of two East Australian Current warm-core eddies, Science 215 (4529), 161-164.

Cresswell, G. and R. Legeckis (1986), Eddies off southeastern Australia, Deep Sea Res. Part A, 33 (11-12), 1527-1562, doi:10.1016/0198-0149(86)90066-X.

Deibel, D., Paffenhofer, G. A. (2009), Predictability of patches of neritic salps and doliolids (Tunicata, Thaliacea). Journal of Plankton Research 31: 1571—1579.

Early, J.J., Samelson, R.M. and Chelton, D.B. (2011), The evolution and propagation of quasigesotrophic ocean eddies. J. Phys. Oceanogr. 41: 1535-1555.

Everett, JD, H. Macdonald, ME Baird, J Humphries, M. Roughan and IM Suthers (2015), Cyclonic entrainment of pre-conditioned shelf waters into a frontal eddy. Journal of Geophysical Research – Oceans 120: 677-6915, doi: 10.1002/2014JC010301

Everett, JD, ME. Baird, PR. Oke, and I. M. Suthers (2012), An Avenue of Eddies: Quantifying the biophysical properties of mesoscale eddies in the Tasman Sea, Geophysical Research Letters, 39, L16608 doi:10.1029/2012GL053091

Everett, J.D., Baird, M.E., Roughan, M., Suthers, I.M., Doblin, M.A. (2014). Relative impact of seasonal and oceanographic drivers on surface chlorophyll a along a Western Boundary Current. Progress in Oceanography 120. (2014) 340–351.

Gaube, P., D. B. Chelton, P. G. Strutton, and M. J. Behrenfeld (2013), Satellite observations of chlorophyll, phytoplankton biomass, and Ekman pumping in nonlinear mesoscale eddies. J. Geophys. Res. Oceans, 118, 6349–6370, doi:10.1002/2013JC009027.

Gaube, P., D. J. McGillicuddy Jr., D. B. Chelton, M. J. Behrenfeld, and P. G. Strutton (2014), Regional variations in the influence of mesoscale eddies on near-surface chlorophyll, J. Geophys. Res. Oceans, 119, 8195–8220, doi:10.1002/2014JC010111.

Gaube, P., D.B. Chelton, R.M. Samelson, M.G. Schlax and L.W. O'Neill (2015), Satellite Observations of Mesoscale Eddy-Induced Ekman Pumping, J. Physical Oceanography, doi:10.1175/JPO-D-14-0032.1

Gula, J., Molemaker, M. J., & McWilliams, J. C. (2015). Gulf Stream dynamics along the southeastern U.S. seaboard. Journal of Physical Oceanography, 45(3), 690-715. doi:10.1175/JPO-D-14-0154.1

Gula, J., Molemaker, M. J., & McWilliams, J. C. (2016). Submesoscale dynamics of a Gulf Stream frontal eddy in the South Atlantic Bight. Journal of Physical Oceanography, 46(1), 305-325. doi:10.1175/JPO-D-14-0258.1

Hetland, R. (2016) Suppression of baroclinic instabilities in buoyancy driven flow over sloping bathymetry. Accepted J. Physical Oceanography doi: http://dx.doi.org/10.1175/JPO-D-15-0240.1

James, C., M. Wimbush, and H. Ichikawa (1999), Kuroshio Meanders in the East China Sea. J. Physical Oceanography 29:2, 259-272.

Joyce, T., R. Backus, K. Baker, P. Blackwelder, O. Brown, T. Cowles, R. Evans, G. Fryxell, D. Mountain, D. Olson, R. Schlitz, R. Schmitt, P. Smith, R. Smith, and P. Wiebe, (1984), Rapid evolution of a Gulf Stream warm core ring. Nature, 308, 837-840

Kasai, A. Kimura, S. Nakata, H. and Okazaki, Y. (2002), Entrainment of coastal water into a frontal eddy of the Kuroshio and its biological significance. J Mar. Sys. 37:185-198.

Kimura, S., Kasai, A., Nakata, H., Sugimoto, T., Simpson, J.H., Cheok, J.V.S., (1997), Biological productivity of mesoscale eddies caused by frontal disturbances in the Kuroshio. ICES Journal of Marine Science 54, 179–192.

Klocker, A., Marshall, D.P., Keating, S.R. and Read, P.L. (2016), A regime diagram for ocean geostrophic turbulence. Q.J.R. Meteorol. Soc., 142 (699): 2411-2417. doi:10.1002/qj.2833

Lee, T. N., J. A. Yoder, and L. P. Atkinson (1991), Gulf Stream frontal eddy influence on productivity of the southeast U.S. continental shelf, J. Geophys. Res., 96(C12), 22191–22205, doi:10.1029/91JC02450.

Macdonald, H. S., Roughan, M., Baird, M.E. and Wilkin, J. (2016), The formation of a cold-core eddy in the East Australian Current. Continental Shelf Res. doi:10.1016/j.csr.2016.01.002

Mahadevan, A. and Tandon, A. 2006. An analysis of mechanisms for submesoscale vertical motions at ocean fronts. Ocean Modelling 14(3): 241-256.

Mahadevan A, D'Asaro E, Lee C, Perry MJ. 2012. Eddy-driven stratification initiates North Atlantic Spring phytoplankton blooms. Science 337:54–58

Mahadevan, A. (2016), The Impact of Submesoscale Physics on Primary Productivity of Plankton. Annu. Rev. Mar. Sci. 2016. 8:17.1–17.24 doi: 10.1146/annurev-marine-010814-015912

Masumoto, Y. Sasaki, H. Kagimoto1, T. Komori, N. Ishida, A., Sasai1, Y., Miyama, T. Motoi1, T. Mitsudera, H. Takahashi, K. Sakuma, H. and T. Yamagata (2004), A fifty-year eddy-resolving simulation of the world ocean: Preliminary outcomes of OFES (OGCM for the Earth Simulator), J. Earth Simul., 1, 35–56.

Mata, M. M., S. Wijffels, J. Church, and M. Tomczak (2006), Eddy shedding and energy conversions in the East Australian Current, J. Geophys. Res., 111, C09034, doi:10.1029/2006JC003592.

Matis PA, WF Figueira, IM Suthers, J Humphries, A Miskiewicz, RA Coleman, B Kelaher and MD Taylor (2014), Cyclonic entrainment? The ichthyoplankton attributes of three major water mass types generated by the separation of the East Australian Current. ICES J. Marine Science 71: 1696-1705.

McDougall, T.J. and P.M. Barker, (2011), Getting started with TEOS-10 and the Gibbs Seawater (GSW) Oceanographic Toolbox, 28pp., SCOR/IAPSO WG127, ISBN 978-0-646-55621-5.

McGillicuddy, D.J., Johnson, R., Siegel, D.A., Michaels, A.F., Bates, N.R., Knap, A.H., (1999), Mesoscale variations of biogeochemical properties in the Sargasso Sea. JGR: Oceans 104 (C6), 13,381–13,394.

McGillicuddy Jr., D.J, L. Anderson, N. R. Bates, T. Bibby, K. O. Buesseler, C. A. Carlson, C. S. Davis, C. Ewart, P. G. Falkowski, S. A. Goldthwait, D. A. Hansell, W. J. Jenkins, R. Johnson, V. K. Kosnyrev, J. R. Ledwell, Q. P. Li, D. A.

Siegel, D. K. Steinberg. (2007), Eddy/Wind Interactions Stimulate Extraordinary Mid-Ocean Plankton Blooms. Science, 316 no. 5827 pp. 1021-1026, DOI: 10.1126/science.1136256.

McWilliams, J.C (1985). A uniformly valid model spanning the regimes of geostrophic and isotropic, stratified turbulence: Balanced turbulence. J. Atmos. Sci. 42: 1773-1774.

McWilliams, J.C. (2016). Submesoscale currents in the ocean. Proc. R. Soc. A 472: 20160117

Mullaney T, and IM Suthers (2013), Entrainment and retention of the coastal larval fish assemblage by a short-lived, submesoscale, frontal eddy of the East Australian Current. Limn. & Oceanography 58: 1546–1556 http://dx.doi.org/10.4319/lo.2013.58.5.1546

Nagai, T., N. Gruber, H. Frenzel, Z. Lachkar, J. C. McWilliams, and G.-K. Plattner (2015), Dominant role of eddies and filaments in the offshore transport of carbon and nutrients in the California Current System, J. Geophys. Res. Oceans, 120, 5318–5341, doi:10.1002/2015JC010889.

Nencioli, F., V.S. Kuwahara, T.D. Dickey, Y.M. Rii, and R.R. Bidigare (2008), Physical dynamics and biological implications of a mesoscale eddy in the lee of Hawai'i: Cyclone Opal observations during E-Flux III. Deep-Sea Research 55: 1252–1274.

Oke, P.R. and Griffin, D.A. (2011). The cold-core eddy and strong upwelling off the coast of New South Wales in early 2007. Deep-Sea Research II 58: 574-591.

Pearce, A. (1981), Temperature-Salinity Relationships in the Tasman Sea. Commonwealth Scientific and Industrial Research Organization, Marine Laboratories Cronulla, N.S.W Technical Report 135.

Ridgway, K. R., R. C. Coleman, R. J. Bailey, and P. Sutton, (2008): Decadal variability of East Australian Current transport inferred from repeated high-density XBT transects, a CTD survey and satellite altimetry. J. Geophys. Res., 113, C08039, doi:10.1029/2007JC004664.

Rubio, A., Barnier, B., Jordà, G., Espino, M., Marsaleix, P., (2009). Origin and dynamics of meso scale eddies in the Catalan Sea (NW Mediterranean): Insight from a numerical model study. J. Geophys. Res. 114 (C6), C06009.

Rykova, T., and P. R. Oke (2015), Recent freshening of the East Australian Current and its eddies, Geophys. Res. Lett., 42, 9369–9378, doi:10.1002/2015GL066050.

Syahailatua, A. Roughan, M. and I. M. Suthers. (2011). Characteristic ichthyoplankton taxa in the separation zone of the East Australian Current: larval assemblages as tracers of coastal mixing. Deep Sea Research II (2011), doi:10.1016/j.dsr2.2010.10.004

Schaeffer, A., M. Roughan, J. E. Wood (2014), Observed bottom boundary layer transport and uplift on the continental shelf adjacent to a western boundary current, J. Geophys. Res. Oceans, 119, doi:10.1002/2013JC009735

Schaeffer, A., A. Gramoulle, M. Roughan , A. Mantovanelli, (2016), Characterizing frontal eddies along the East Australian Current from HF radar observations. Submitted to JGR - Oceans

Schiller, A., P. R. Oke, G. B. Brassington, M. Entel, R. Fiedler, D. A. Griffin, and J. V. Mansbridge, (2008), Eddy-resolving ocean circulation in the Asian-Australian region inferred from an ocean reanalysis effort. Progress in Oceanography, 76, 334-365.

Siegel, D. A., P. Peterson, D. J. McGillicuddy Jr., S. Maritorena, and N. B. Nelson (2011), Biooptical footprints created

by mesoscale eddies in the Sargasso Sea, Geophys. Res. Lett., 38, L13608, doi:10.1029/2011GL047660

Stammer, D. (1997), Global characteristics of ocean variability estimated from regional TOPEX/Poseidon altimeter measurements, J. Phys. Oceanogr., 27, 1743–1769.

Thomas, L. N., J. R. Taylor, R. Ferrari, and T. M. Joyce, (2013). Symmetric instability in the Gulf Stream, Deep Sea Res. II, 91, 96-110.

Thomas, L. N., A. Tandon, and A. Mahadevan, (2008). Sub-mesoscale processes and dynamics. In M. W. Hecht, and H. Hasumi (Eds.), Ocean Modeling in an Eddying Regime, Geophysical Monograph Series, Volume 177, American Geophysical Union, Washington DC, pages 17-38.

Thurnherr, A. M. (2010), A practical assessment of uncertainties in full-depth velocity profiles obtained with Teledye/RDI Workhorse Acoustic Doppler Current Profilers, J. Atm. Oc. Tech. 27, 1215-1227.

Valladeau, G. P. Thibaut, B. Picard, J. C. Poisson, N. Tran, N. Picot & A. Guillot (2015), Using SARAL/AltiKa to Improve Ka-band Altimeter Measurements for Coastal Zones, Hydrology and Ice: The PEACHI Prototype, Marine Geodesy, 38:sup1, 124-142, DOI: 10.1080/01490419.2015.1020176

Verron, J. P. Sengenes, Juliette Lambin, Jocelyne Noubel, Nathalie Steunou, Amandine Guillot, Nicolas Picot, Sophie Coutin-Faye, Rashmi Sharma, R. M. Gairola, D. V. A. Raghava Murthy, James G. Richman, David Griffin, Ananda Pascual, Frédérique Rémy & P. K. Gupta (2015), The SARAL/AltiKa Altimetry Satellite Mission, Marine Geodesy, 38:sup1, 2-21, DOI: 10.1080/01490419.2014.1000471

Wilkin, J., and W. Zhang (2007), Modes of mesoscale sea surface height and temperature variability in the East Australian current, J. Geophys. Res., 112, C01013, doi:10.1029/2006JC003590.

Wood, J.E., Schaeffer, A., Roughan, M., P.M. Tate (2016), Seasonal variability in the continental shelf waters off southeastern Australia: fact or fiction? Continental Shelf Research 112, 92-103 doi:10.1016/j.csr.2015.11.006

Yoder, J., L. Atkinson, T. Lee, H. Kim, and C. McClain, (1981), Role of Gulf Stream frontal eddies in forming phytoplankton patches on the outer southeastern shelf. Limnol. Oceanogr., 26, 1103–1110, doi:10.4319/lo.1981.26.6.1103.

Yoshida, S., Qiu, B., Hacker, P. (2010), Wind-generated eddy characteristics in the lee of the island of Hawaii. J. Geophys. Res., 115, C03019.

Zhang, Z. W. Wang, B. Qiu (2014), Oceanic mass transport by mesoscale eddies. Science 345, 322; doi: 10.1126/science.1252418

Table Captions

Table 1: Metadata for all the CTD casts undertaken during the Cruise.

Table 2: Meta data for the NOAA drifters that were deployed inside Murphy (D1-D3) and Freddy (D4-D6). Distances in brackets under release location indicate the number of kilometers either north or south of the approximate eddy center that the drifter was released.

Table 3: Summary of the physical characteristics of the two eddies (Murphy and Freddy) attributed to the observation used to make the calculation.

Table 4: Eddy Centre Estimates for Freddy and Murphy calculated from shipboard ADCP data using the method of closest approach. Duration indicates the time period of the ADCP data used to estimate the eddy centre.

Figure Captions

Figure 1: (a) 3 day composite SST and geostrophic velocities derived from SSH centred on 7 June 2016. MODIS SST (b) and Ocean Color (c) for Murphy (5 Jun 2015), top and Freddy (9 June 2015) bottom. Solid black lines indicate the location of the ADCP and Triaxus lines in subsequent figures. (d) and (e) are zoom insets (as indicated in b and c) of cruise track colored by SST from the underway thermosalinograph, velocities at 30 m depth as measured by the shipboard ADCP and the location of CTD casts (numbered circles). Bathymetric contours are 4000, 2000, 200, 100 m from east to west.

Figure 2: Shipboard ADCP current measurements in the top ADCP bin in Eddy Murphy. At each grid point, the mean radial and tangential velocities about this point is calculated by averaging over all ADCP measurements. The contours show points with the same mean tangential velocity. The red dashed lines show points with zero radial velocity. The green circle shows the estimated eddy center location (zero radial velocity, maximum mean tangential velocity).

Figure 3: (a) The tangential velocity about the eddy center is related to the normal (across-track) and longitudinal (along-track) velocities using the angle subtended by the distance along the ship track from the point of closest approach to the eddy center. (b) Shipboard ADCP current measurements over a three-hour period on 5 June 2015 as the ship passed the center of the large northern eddy (Murphy). The colour scale indicates time in UTC (hours). The estimated eddy center is shown in red with 95% confidence interval. (c) Normal and longitudinal velocity components as a function of distance along the ship track. Blue and red lines indicate the least-squares fits with 95% confidence intervals.

Figure 4. a) Trajectories of drifters released inside Murphy, D1 (blue, center), D2 (green, north of center) and D3 (red, south of center). See Table 2 for drifter release details. Color-coded dots indicate the last position of the drifter used for analysis (presumed to be while the drifter remained inside the eddy), and lighter colored lines are used to show the rest of the trajectory (presumed to be once the drifter was outside the eddy). b-d) Trajectories of drifters released inside Murphy showing the dates (colorbar) when drifter positions were recorded; black dots indicate the last position of the drifter used for analysis. e) Trajectories of drifters released inside Freddy, D4 (blue, center), D5

(green, north of center) and D6 (red, south of center). See Table 2 for drifter release details. Color-coded dots indicate the last position of the drifter used for analysis (presumed while the drifter remained inside the eddy), and lighter colored lines are used to show the rest of the trajectory (presumed to be once the drifter was outside the eddy). D5 remained inside the eddy throughout the trajectory. f-h)Trajectories of drifters showing the dates (colorbar) when drifter positions were recorded; black dots indicate the last position of the drifter used for analysis.

Figure 5: a) Velocity from shipboard ADCP (to 800 m), normal to the ships track, bold contour is +/- 0.5ms^{-1}, contour interval is 0.1ms^{-1} b) temperature from the Triaxus (to 150 m), with practical salinity contours (black, contour interval = 0.05) c) steric height anomaly, relative to a reference level of 140 m, and d) Brunt-Väisälä Frequency Squared (N^2) e) chlorophyll *a* fluorescence from the Triaxus. The location of each transect is identified in Figure 1 for Murphy (left) south to north and Freddy (right), west to east. Spacing between CTD casts is 900 - 1500m.

Figure 6: Hydrographic transects from CTD profiles through Murphy (Left) and Freddy (Right). Top: Temperature (colour) and salinity contours. Middle: chlorophyll *a* (colour) and density contours. Bottom: Dissolved oxygen (colour) with spice contours. A stretched view of the CTD profiles that shows the uplift more clearly is shown in the Sup. Mat. Figures 6 and 7.

Figure 7: T-S Density diagrams coloured by depth (left) dissolved oxygen (middle) and fluorescence (right) to a depth of 250 m for CTD casts 20, (Freddy core), 23, (southern mixed edge of Freddy) and 26 (northern 'EAC' edge of Freddy).

Figure 8: Transects of nutrients through Murphy (left) and Freddy (right). Row 1: contours of temperature, coloured by nitrate, Row 2: contours of density, coloured by phosphate. Row 3: contours of oxygen, coloured by silicate, Row 4, contours of chlorophyll *a*, coloured by ammonia. For Murphy (left) and Freddy (right).

Figure 9: (a) Ship track over a 51 hour period from June 4-6. The centre of eddy Murphy on 5 June 03:30 and 5 June 16:00 is indicated by pink circles. The colour scale shows sea-surface temperature from MODIS SST imagery on 5 June 07:01. For comparison, the underway temperature is shown in the filled circles. The large red patch in the SW corner is due to cloud cover. The green dots show ground track of the SARAL satellite on 2 June 20:01. (b) Ship track over a 21.5 hour period from June 9 - 10. Pink circles indicate eddy center estimates for Freddy on 9 June 00:15 and 16 June 16:00. The colour scale shows sea-surface temperature from MODIS SST imagery on 08:01 June 8 (note the different colour scales and axis ranges in a and b). The large blue patch in the southern part of the image is a mesoscale cyclonic eddy. Green dots show the ground track of the SARAL satellite on 8 June 20:12, by which time the core of the eddy had moved slightly.

Figure 10 (*a*) Zonal (west-east) displacement of the centre of Murphy (black circles) and 95% confidence intervals (horizontal black lines) as functions of depth. The blue line and 95% confidence interval shows a weighted least squares fit to a linear zonal tilt. (*b*) Meridional (north-south) tilt of the Murphy. The red line and 95% confidence interval shows the weighted least squares fit to a linear meridional tilt. (*c*) Zonal and (d) meridional tilt of Freddy.

Figure 11: Rotation period (T) and Rossby number (Ro) inferred from shipboard ADCP as a function of depth for the Murphy (in red) and Freddy (blue). The shaded regions indicate the 95% confidence intervals.

Figure 12. (a) Schematic showing the projection of a Gaussian eddy velocity profile (estimated from ADCP data) projected onto the satellite groundtrack. (b) Estimates of the geostrophic (Coriolis), non-geostrophic (centripetal) and the total (sum of both) contributions to the sea-level anomaly for a Gaussian eddy, compared to the sea level anomaly as measured by the Altika altimeter from a pass over Murphy. Vertical dashed lines indicate the e-folding lengthscale of the eddy as measured along the satellite groundtrack. (c) As in (b) for Freddy. The Altika groundtracks are indicated in Figure 9.

Figure 13: (a) Comparison of the measured tangential velocity versus the velocity expected from uniform vorticity flow at all depths in Eddy Murphy. Different sectors of the eddy are indicated by the color shading. The diagonal line indicates the line of uniform rotation and separates regions where the tangential velocity is faster or slower than the rotation of the eddy core. Negative tangential velocities indicate anti-cyclonic rotation. (b) Same as in Freddy.

Figure 1.

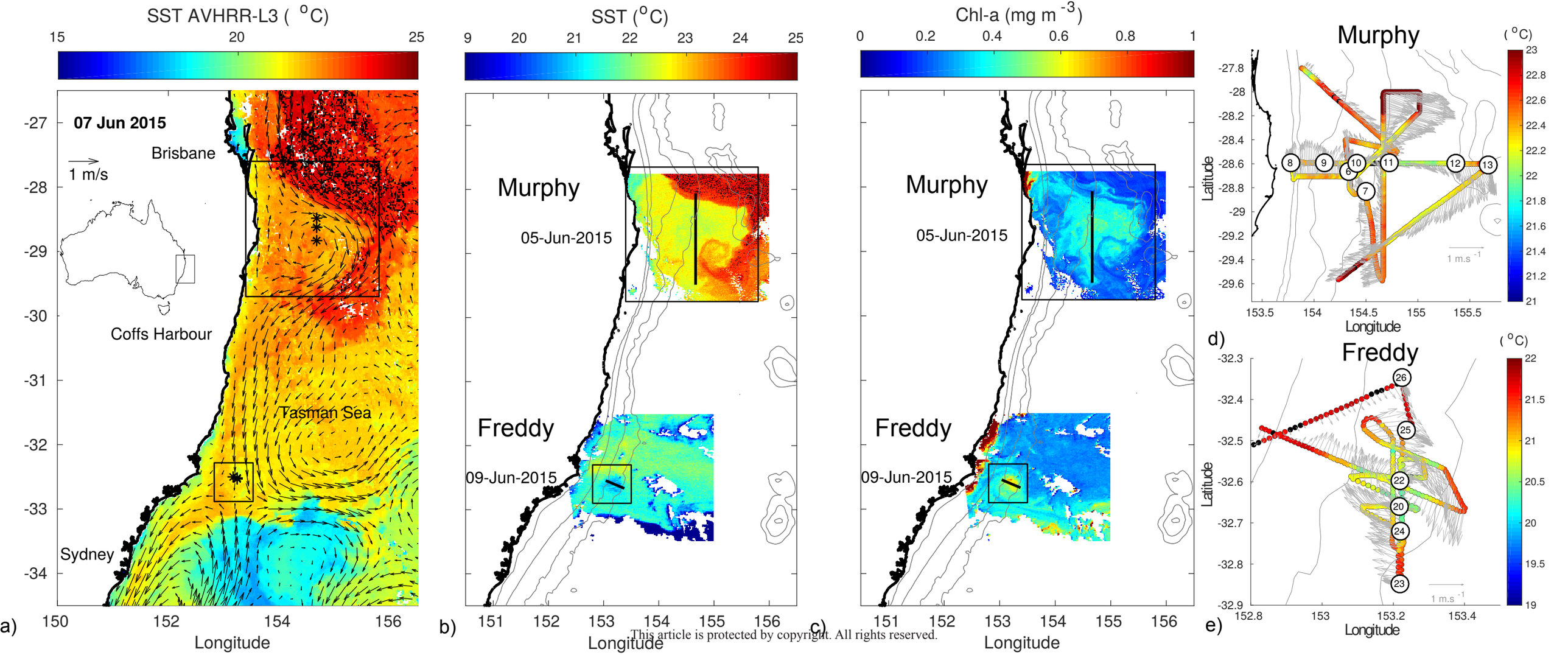

Figure 2.

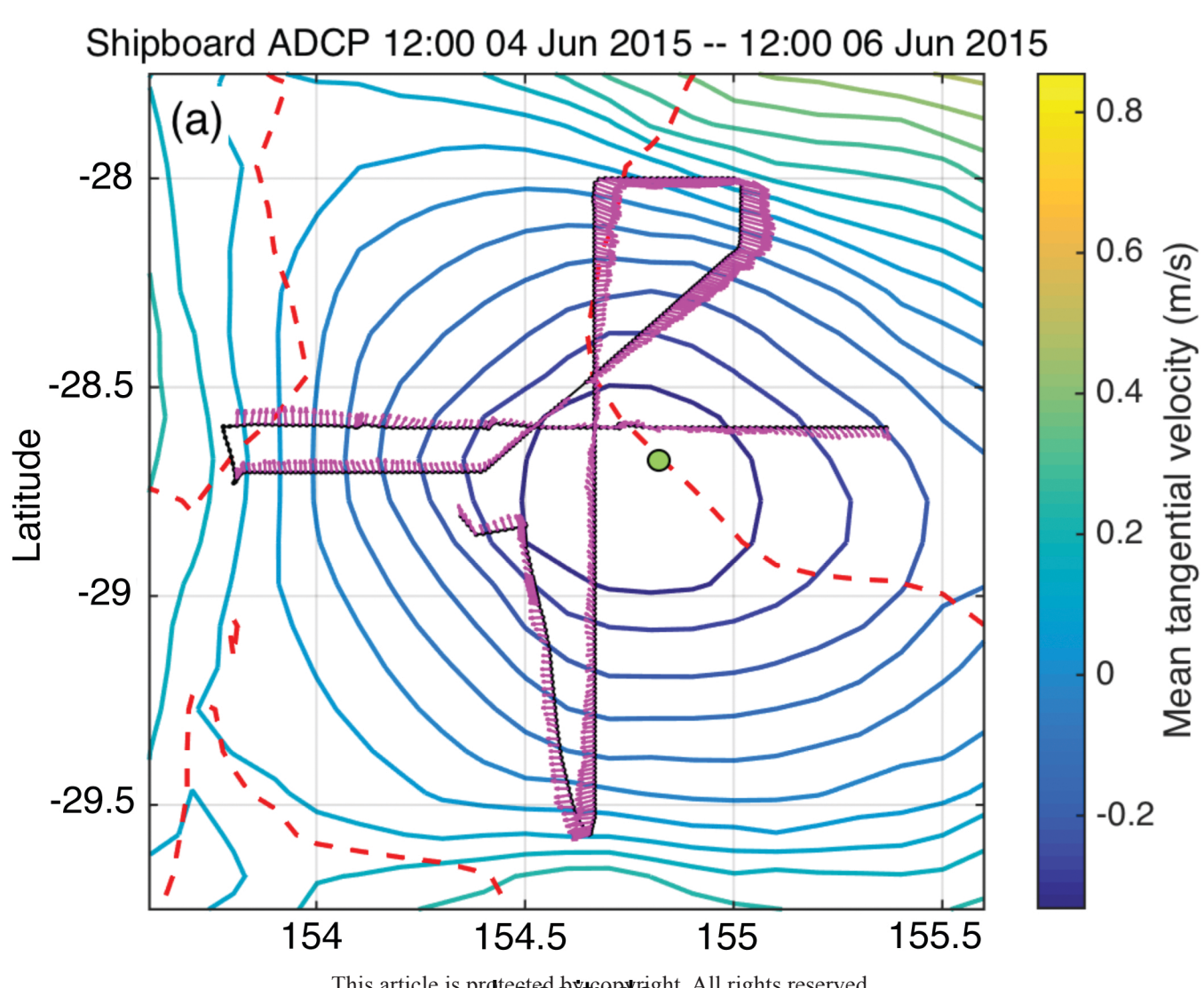

Figure 3.

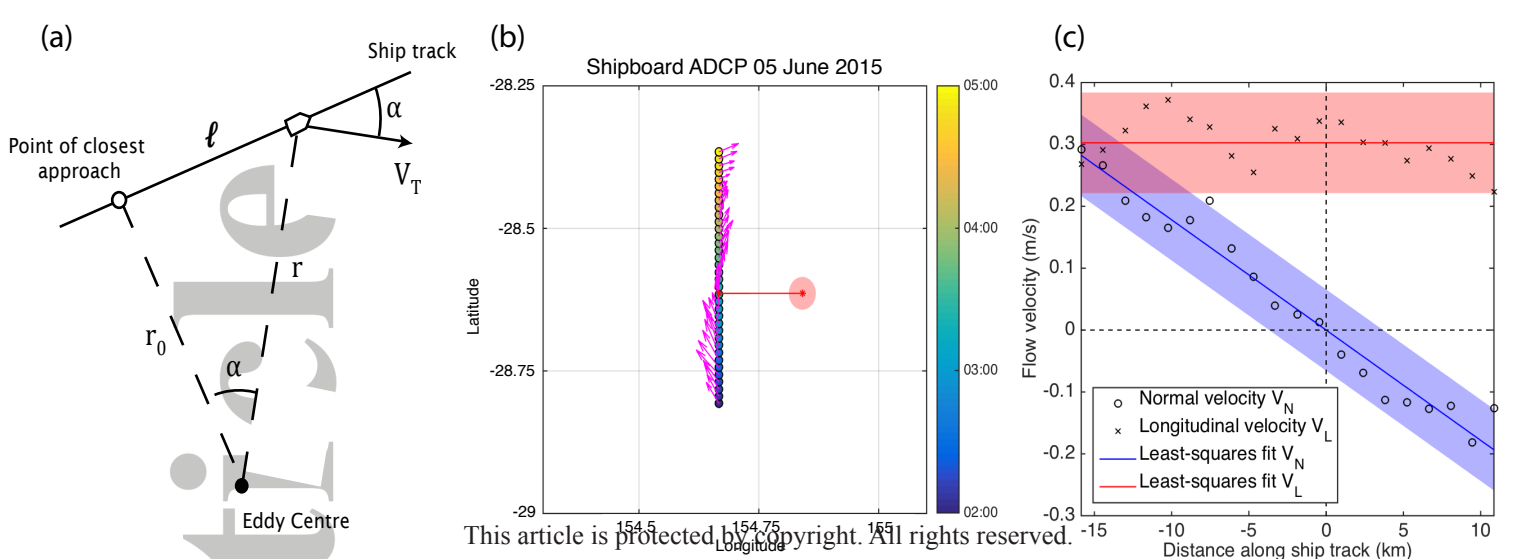

Figure 4.

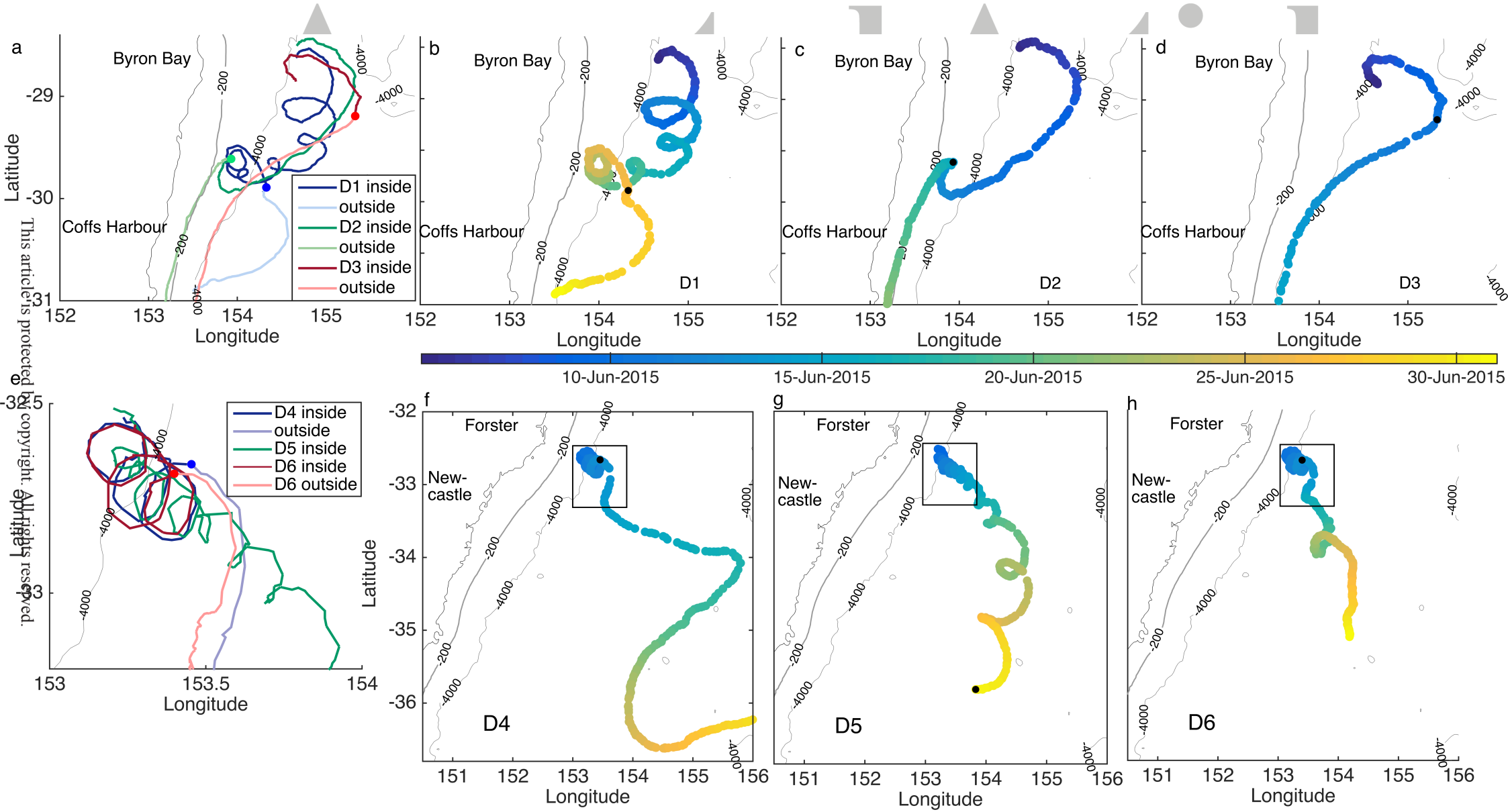

Figure 5.

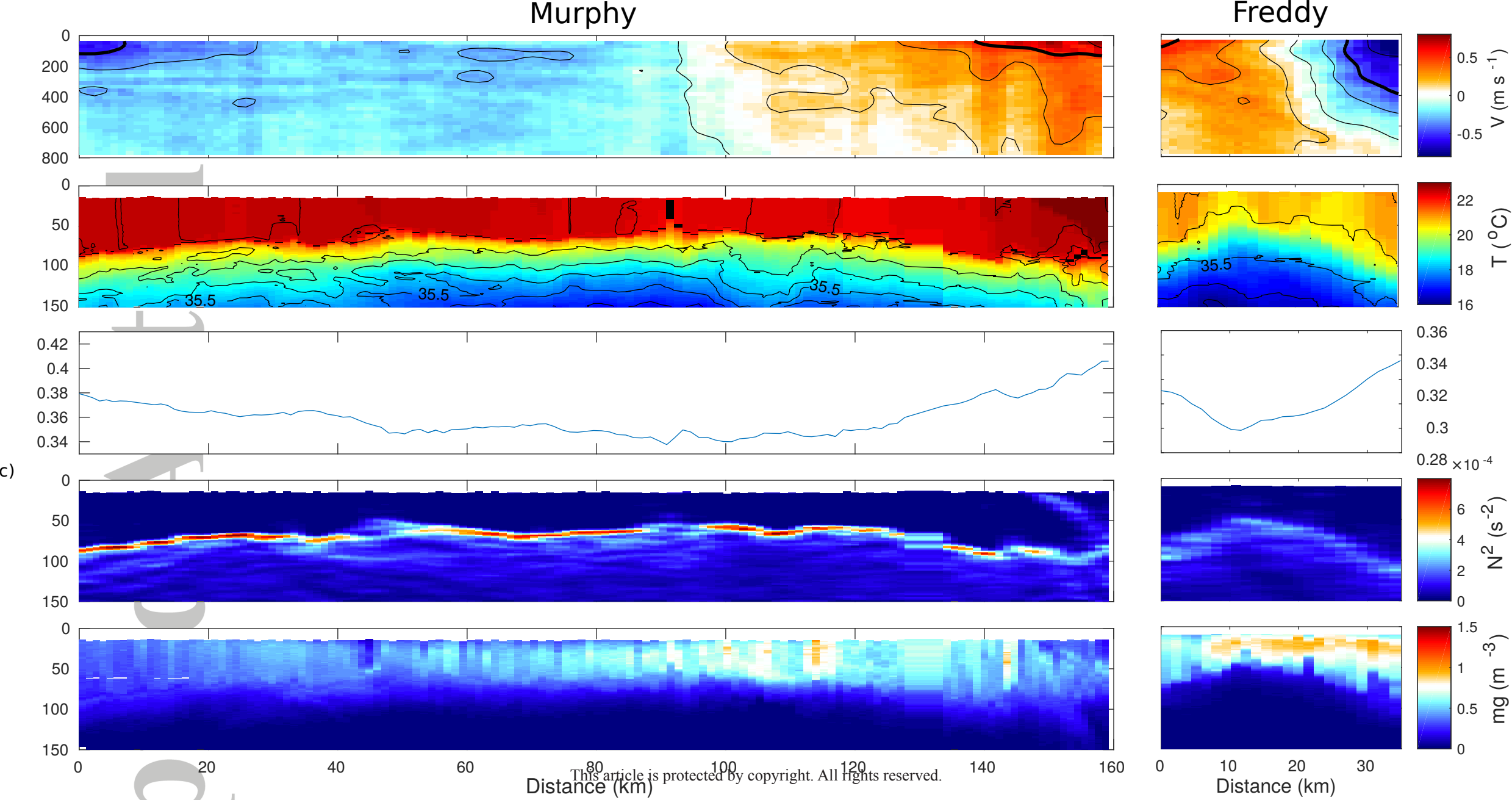

Figure 6.

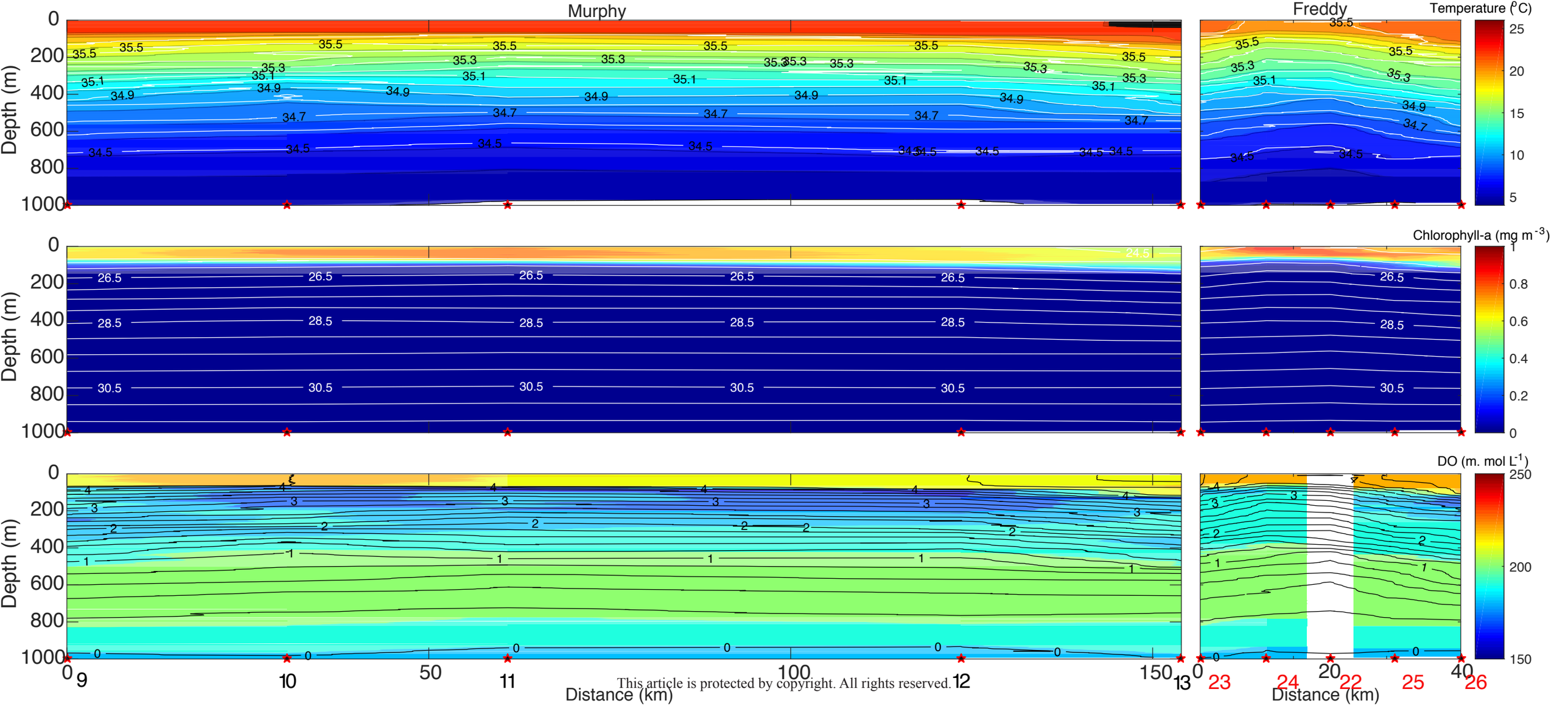

Figure 7.

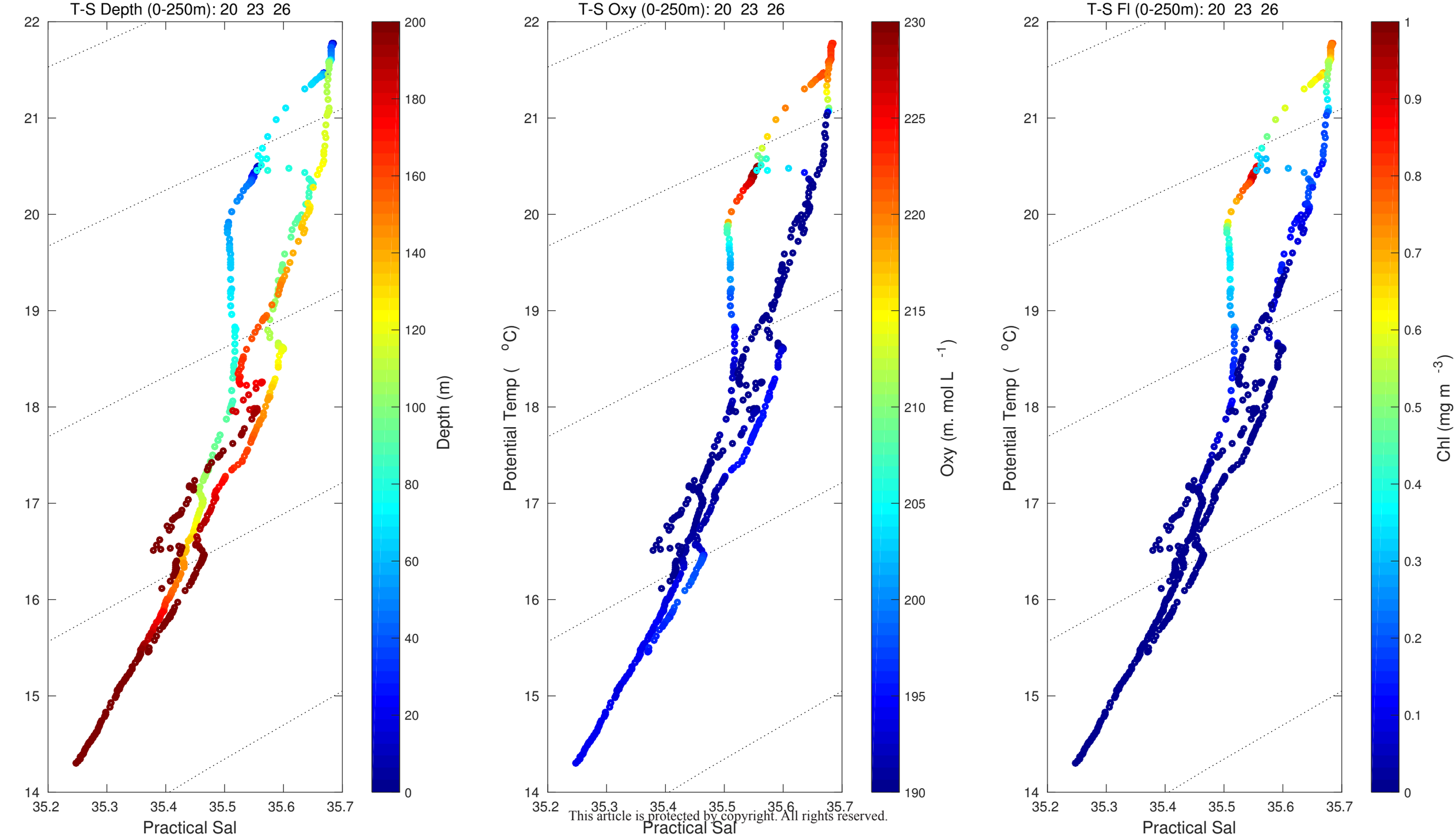

Figure 8.

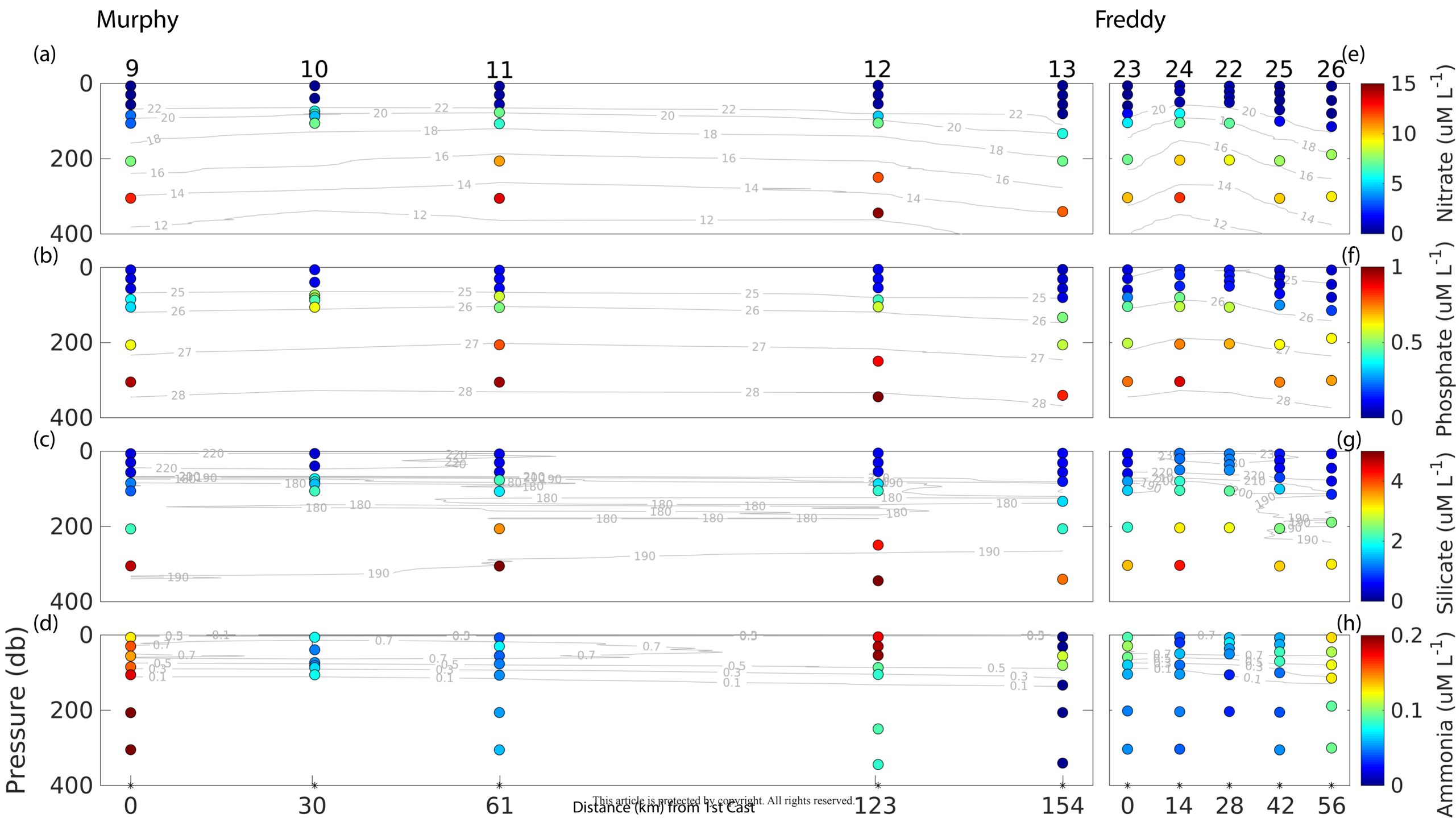

Figure 9.

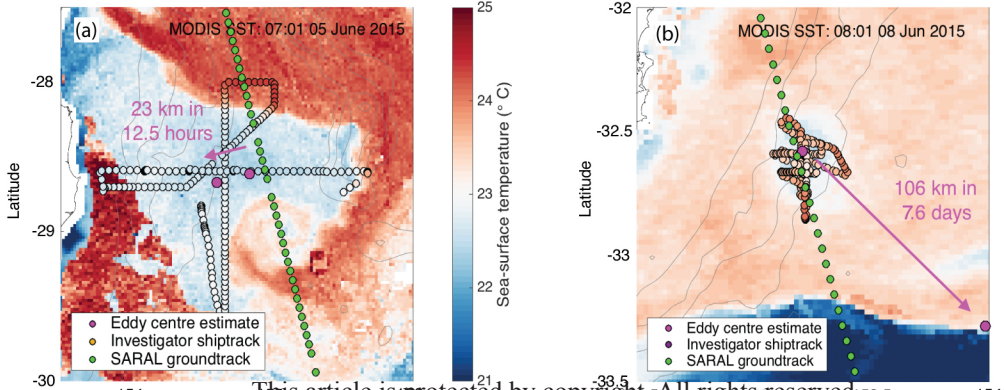

Figure 10.

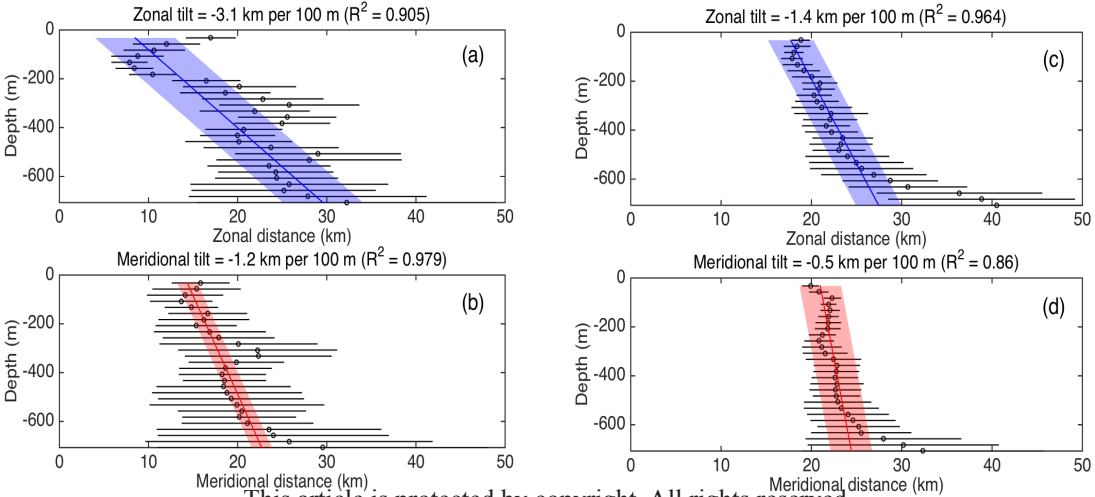

Figure 11.

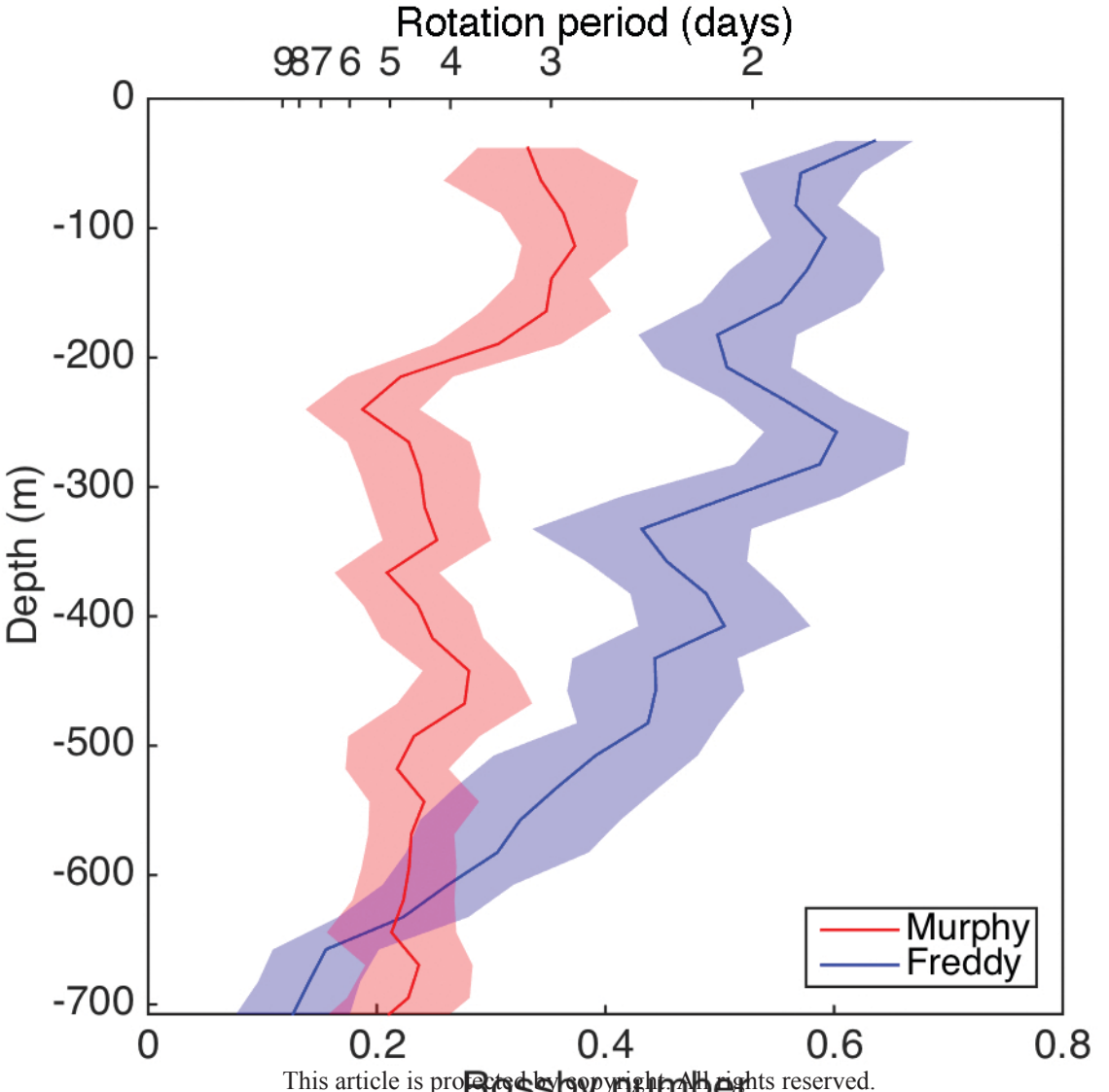

Figure 12.

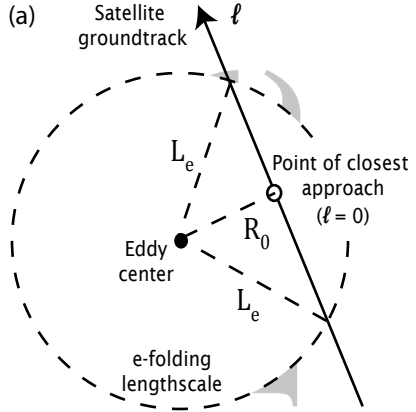

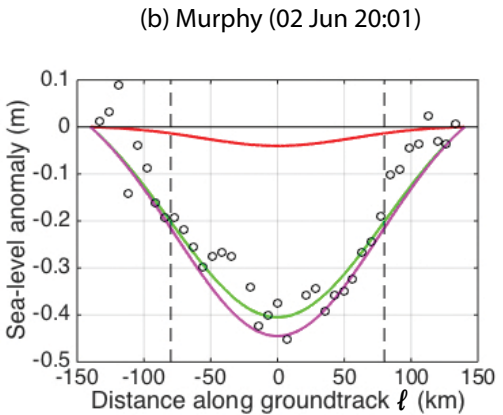

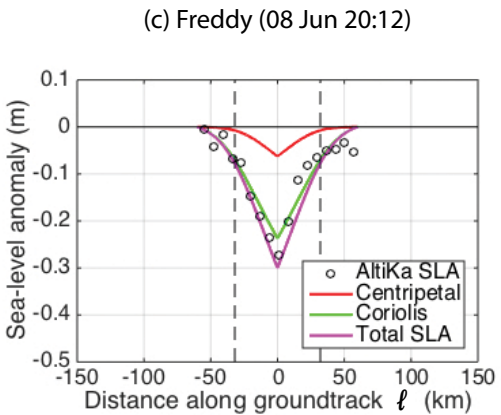

Figure 13.

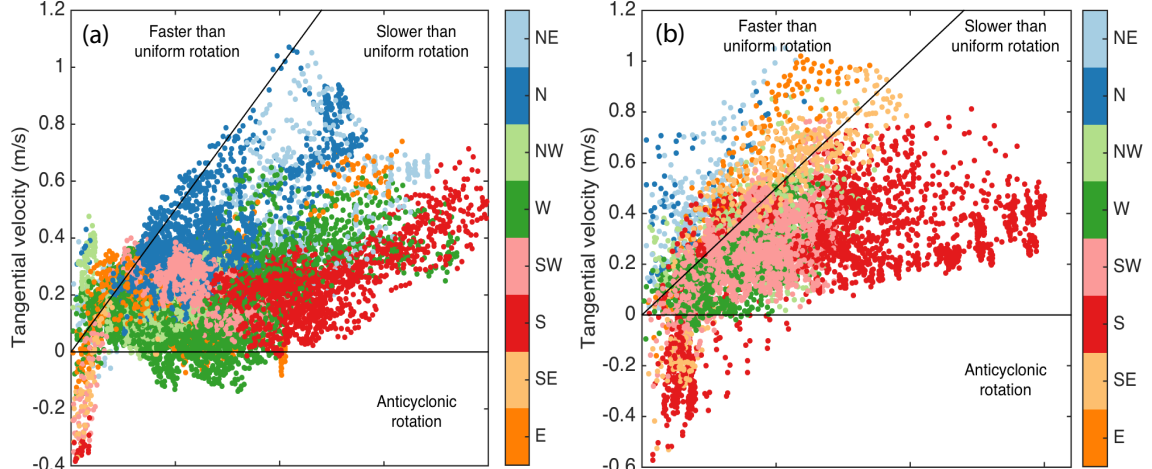

Cast No.	Date (dd/mm/yy)	Time (UTC)	Lat (Deg S)	Long (Deg E)	Cast Depth	Water Depth
2	03/06/15	07:30:03	-26.983	153.880	998	1503
4	03/06/15	10:17:13	-26.982	153.880	504	1525
5	03/06/15	20:41:12	-27.718	153.770	108	123
6	04/06/15	08:08:56	-28.664	154.340	506	2842
7	04/06/15	13:24:32	-28.829	154.500	504	3375
8	05/06/15	22:50:56	-28.592	153.780	78	88
9	06/06/15	01:41:53	-28.592	154.100	999	2220
10	06/06/15	04:34:22	-28.595	154.410	1003	4048
11	06/06/15	07:57:48	-28.591	154.730	1008	4704
12	06/06/15	12:26:27	-28.598	155.370	1003	4110
13	06/06/15	15:22:08	-28.609	155.680	991	3243
14	07/06/15	04:13:58	-30.023	153.560	320	327
15	07/06/15	05:30:08	-30.028	153.570	769	796
16	07/06/15	07:28:46	-30.026	153.580	1243	1210
17	07/06/15	10:36:02	-30.037	153.610	1463	1552
18	07/06/15	19:51:24	-30.056	153.650	77	2213
19	07/06/15	21:40:21	-30.049	153.650	2241	2173
20	09/06/15	11:47:21	-32.661	153.220	497	3207
22	09/06/15	20:21:37	-32.596	153.220	1001	2986
23	09/06/15	23:08:33	-32.849	153.220	1005	4450
24	10/06/15	01:19:58	-32.720	153.220	1009	3763
25	10/06/15	04:06:01	-32.474	153.240	993	3515
26	10/06/15	06:08:23	-32.347	153.220	986	2867
27	10/06/15	11:30:43	-32.499	152.700	100	114
28	10/06/15	21:09:28	-32.055	152.970	107	122
29	11/06/15	01:10:20	-32.598	153.050	1005	1826
30	11/06/15	03:01:30	-32.592	153.130	995	2392
31	11/06/15	04:39:30	-32.595	153.180	997	2660
32	11/06/15	06:27:52	-32.599	153.290	1001	3346
33	11/06/15	08:08:43	-32.602	153.360	1006	3986
34	11/06/15	09:44:07	-32.603	153.440	995	4654
35	11/06/15	13:48:58	-32.672	153.590	1010	4821
36	11/06/15	20:33:58	-32.723	153.300	1020	4079
37	12/06/15	13:12:36	-32.750	153.370	507	4377
38	12/06/15	19:39:50	-32.788	153.780	4	4798
39	12/06/15	20:31:04	-32.800	153.790	506	4797
40	12/06/15	09:25:00	-30.620	153.370	6	498
41	13/06/15	22:09:59	-30.621	153.370	470	456
42	13/06/15	21:05:00	-32.000	153.250	1012	1551
43	15/06/15	23:07:00	-32.000	153.160	1008	1066
44	16/06/15	00:48:00	-32.000	153.080	225	239
45	16/06/15	02:18:00	-32.000	152.990	109	119
46	16/06/15	03:32:00	-32.000	152.920	104	116
47	16/06/15	04:55:00	-32.000	152.830	88	98
48	16/06/15	13:49:01	-33.147	153.870	1010	4799

Drifter ID #	UTC release date (2015)	UTC release hour (hh:mm)	Release latitude (Deg S)	Release longitude (Deg E)	Release location	
					Location	Eddy
139658 (D1)	5 June	03:10	-28.625	154.667	Centre	Murphy
139659 (D2)	5 June	04:02	-28.490	154.667	North (15km)	
139657 (D3)	5 June	01:45	-28.836	154.667	South (23km)	
139662 (D4)	9 June	04:00	-32.520	153.249	Centre	Freddy
139663 (D5)	9 June	04:18	-32.508	153.174	North (4km)	
139661 (D6)	9 June	03:42	-32.534	153.249	South (4km)	

		Murphy	Freddy
Birth	Date (2015)	9 May	2 June
Sampling	Date (2015)	4 June	9 June 16 June
Age at sampling	Days	~ 26 days	~7 days
Life Span	SST	~43 days	N/A
	SSH	~42 days (11 May – 1 June)	N/A
	Drifters	~ 47 days (9 May - 26 June)	28 days (2- 30 June)
Diameter	SST	163 km	35 km
	SSH	170 km	N/A
	S-ADCP	156-186 km	19-44 km
	Triaxus (from center of the Eddy)	160 km	>35 km
Depth	CTD (flat isopycnals)	> 1000 m	~1000 m
	S-ADCP	> 800 m	>800 m
	L-ADCP	> 1000 m	~ 1000 m
Tangential Velocity	S-ADCP	0.5 ms^{-1}	0.7 ms^{-1}
Rotation Speed	Drifters	0.44 ms^{-1}	0.5 ms^{-1}
Temperature	SST Anomaly (Deg C)	1.5	2

	UTC Date June 2015	Time	Duration (hours)	Latitude (Deg S)	Longitude (Deg E)
Murphy	5	3:30	3	-28.6168	154.8351
	5	16:00	3	-28.6726	154.6091
Freddy (visit 1)	9	0:15	3	-32.5763	153.2057
	9	3:45	1.5	-32.5825	153.1891
	9	6:35	1.5	-32.5691	153.2188
	9	14:15	1	-32.6099	153.2487
	9	21:45	1.5	-32.655	153.2435
	10	2:45	1	-32.6425	153.2461
	12	16:15	1.5	-32.8224	153.4448
Freddy (visit 2)	16	16:00	1	-33.2769	153.9855
	16	23:30	1	-33.2702	153.8311